PERSPECTIVE

Check for updates

Development of formamidinium lead iodide-based perovskite solar cells: efficiency and stability

Ziwei Zheng,† Shiyu Wang,† Yue Hu, [ID] Yaoguang Rong, [ID] Anyi Mei and Hongwei Han [ID] *

Perovskite materials have been particularly eye-catching by virtue of their excellent properties such as high light absorption coefficient, long carrier lifetime, low exciton binding energy and ambipolar transmission (perovskites have the characteristics of transporting both electrons and holes). Limited by the wider band gap (1.55 eV), worse thermal stability and more defect states, the first widely used methylammonium lead iodide has been gradually replaced by formamidinium lead iodide ($FAPbI_3$) with a narrower band gap of 1.48 eV and better thermal stability. However, $FAPbI_3$ is stabilized as the yellow non-perovskite active phase at low temperatures, and the required black phase (α-$FAPbI_3$) can only be obtained at high temperatures. In this perspective, we summarize the current efforts to stabilize α-$FAPbI_3$, and propose that pure α-$FAPbI_3$ is an ideal material for single-junction cells, and a triple-layer mesoporous architecture could help to stabilize pure α-$FAPbI_3$. Furthermore, reducing the band gap and using tandem solar cells may ulteriorly approach the Shockley–Queisser limit efficiency. We also make a prospect that the enhancement of industrial applications as well as the lifetime of devices may help achieve commercialization of PSCs in the future.

1. Introduction

As one of the most promising emerging photovoltaics, perovskite solar cells (PSCs) have attracted extensive attention and developed rapidly in the past decade for renewable and clean energy.[1–5] Miyasaka *et al.* introduced methylammonium-based halide perovskites, namely, methylammonium lead iodide ($MAPbI_3$) and methylammonium lead bromine ($MAPbBr_3$), into dye-sensitized solar cells as light absorbers for the first time in 2009 and achieved an efficiency of 3.8% at that moment.[6] With the optimization of deposition technology and device configuration,[7–11] PSCs with $MAPbI_3$ perovskites as the light-absorbing layer reached the highest efficiency of 22.28% in 2020.[12] $MAPbI_3$ faces several problems such as poor thermal stability and wider band gap (1.55 eV).[13,14] Formamidinium lead iodide ($FAPbI_3$) perovskites are considered to exhibit higher thermal stability and a more ideal band gap of 1.48 eV.[15,16] The efficiency of $FAPbI_3$-based PSCs prepared for the first time is not high.[17] Snaith *et al.* found that $FAPbI_3$ has sufficiently long electron and hole diffusion lengths for planar heterojunction solar cells to be a suitable configuration.[18] M. Grätzel *et al.* first used FA/MA mixed cationic perovskites, but MA is still the main

ingredient.[19] Park *et al.* formed a thin $MAPbI_3$ overlayer on $FAPbI_3$ to enhance the short-circuit current density.[20] Seok *et al.* stabilized the black phase of $FAPbI_3$ (α-$FAPbI_3$) by introducing $MAPbBr_3$ and obtained a breakthrough for FA-based PSCs.[21] Park *et al.* found that cesium (Cs) can stabilize the black phase of $FAPbI_3$.[22] Furthermore, mixed Cs-MA-FA cation-based devices can achieve a high efficiency of more than 22%.[23–28] Since then, an increasing number of devices have been using FA-based perovskites as the light-absorbing layer and have achieved a higher efficiency.[29,30] $FAPbI_3$-based PSCs have recently obtained a certified efficiency of 25.21%.[31] These results indicate that $FAPbI_3$ shows excellent potential for efficient PSCs.

We have sorted out the annual efficiency growth trends of PSCs with MA-based perovskites (Table 1) and FA-based perovskites (Table 2). The current focus of PSCs is shifting from MA-based ones to FA-based ones (Fig. 1). As the most ideal single-junction light-absorbing material, $FAPbI_3$ with 1.48 eV band gap has displayed the impressive potential. In this work, we focused on the future development direction of PSCs. For single-junction cells, we compared the basic properties of $MAPbI_3$ and $FAPbI_3$. Herein, we summarize the relevant methods for stabilizing α-$FAPbI_3$, and speculate that nano-localization effects may be one of the potential methods to stabilize the pure α-$FAPbI_3$ phase. For other aspects, further narrowing the band gap and developing tandem cells may be another way to achieve or even break the Shockley–Queisser (S–Q) limit. Besides, we simply summarize the development of Sn–Pb and tandem solar cells and discuss the current problems. In

Michael Grätzel Center for Mesoscopic Solar Cells, Wuhan National Laboratory for Optoelectronics, Key Laboratory of Materials Chemistry for Energy Conversion and Storage of Ministry of Education, Huazhong University of Science and Technology, Wuhan, 430074, Hubei, PR China. E-mail: hongwei.han@mail.hust.edu.cn

† These authors contributed equally to this work.

Table 1 Annual efficiency process of MAPbI$_3$

Year	Main composition	V_{oc} (mV)	J_{sc} (mA cm^{-2})	FF	PCE (%)	Ref.
2009	MAPbI$_3$	610	11.00	0.570	3.81	6
2011	MAPbI$_3$	706	15.82	0.586	6.54	32
2012	MAPbI$_3$	888	17.60	0.620	9.70	1
2013	MAPbI$_3$	980	17.80	0.630	10.90	33
2013	MAPbI$_3$	1020	18.00	0.670	12.30	2
2014	MAPbI$_3$	1130	22.75	0.751	19.30	7
2015	MAPbI$_3$	1086	23.83	0.762	19.71	8
2016	MAPbI$_3$	1113	23.69	0.773	20.40	9
2017	MAPbI$_3$	1120	23.40	0.813	21.30	10
2018	MAPbI$_3$	1100	22.70	0.810	20.20	11
2019	MAPbI$_3$	1120	23.23	0.814	21.17	34
2020	MAPbI$_3$	1159	24.11	0.797	22.28 (certified)	12

Table 2 Annual efficiency process of FAPbI$_3$

Year	Main composition	V_{oc} (mV)	J_{sc} (mA cm^{-2})	FF	PCE (%)	Ref.
2013	FAPbI$_3$	970	6.45	0.687	4.30	17
2014	FAPbI$_3$	1032	20.97	0.740	16.01	20
2015	FAPbI$_3$	1059	24.65	0.770	20.11 (certified)	35
2016	FAPbI$_3$	1134	23.70	0.780	21.02 (certified)	36
2017	FAPbI$_3$	1100	25.00	0.803	22.10 (certified)	37
2018	FAPbI$_3$	1080	25.06	0.755	20.35	38
2019	FAPbI$_3$	1144	26.70	0.776	23.69 (certified)	27
2020	FAPbI$_3$	1181	26.18	0.796	24.64 (certified)	39
2021	FAPbI$_3$	1174	26.25	0.818	25.21 (certified)	31

order to realize the industrialization of PSCs, it is very important to realize the preparation of perovskite solar cells in the air. We summarize some successful cases of preparation in the air and put forward several prospects.

2. A promising photovoltaic material of FAPbI$_3$

2.1 Inherent properties

Perovskite crystals have a general ABX$_3$ chemical formula. The ions at the A site are MA$^+$, FA$^+$ or Cs$^+$; the ions at the B site are
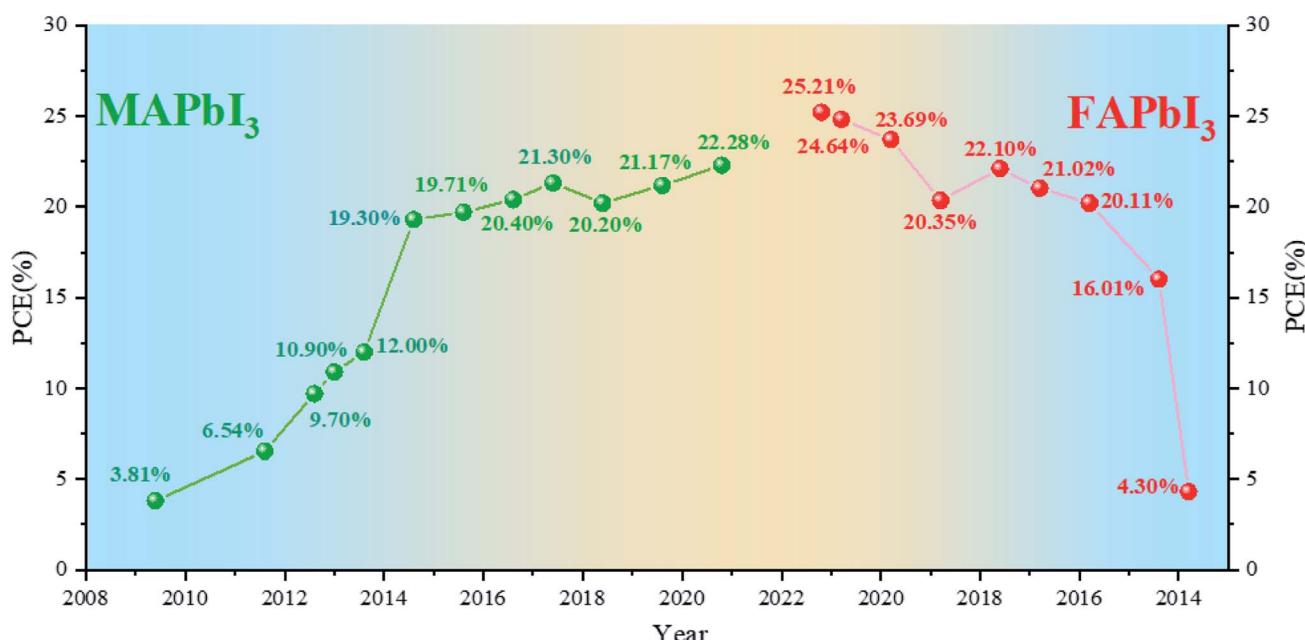
Fig. 1 Development of MA-based and FA-based perovskite solar cells.

Pb^{2+} or Sn^{2+}; and the ions at the X site are I$^-$, Br$^-$ or Cl$^-$, as shown in Fig. 2a. The A, B and X ions satisfying the Goldschmidt equation are a prerequisite to form a perovskite structure.[40] As the first used material in PSCs, MAPbI$_3$ has been widely employed due to its excellent photovoltaic performance. However, it has been gradually discovered that the larger band gap, lower charge-carrier mobility and more defect state density of MAPbI$_3$ limit its further improvement in efficiency.[7,41–43] At the same time, since MA cations are thermally unstable, the stability of the MAPbI$_3$ perovskite has always been a problem.[44] In 2013, Tom et al. introduced FA into PSCs for the first time,

allowing FA cations to enter researchers' field of vision.[17] Compared with the lower tolerance factor of 0.91 for MAPbI$_3$, FAPbI$_3$ has a higher tolerance factor of 0.99,[45] which is more close to the upper limit of the tolerance factor, and this indicates a perfect fit (Fig. 2b).[46] Meanwhile, while maintaining the same band structure and absorption coefficient, FAPbI$_3$ has a narrower band gap than that of MAPbI$_3$ (Fig. 2c), and it is more likely to achieve a more efficient solar cell.[18] Starting from the physical properties of the material itself, we systematically compared the physical properties of the two materials. The effective masses of holes and electrons of MAPbI$_3$ are 0.19m_e
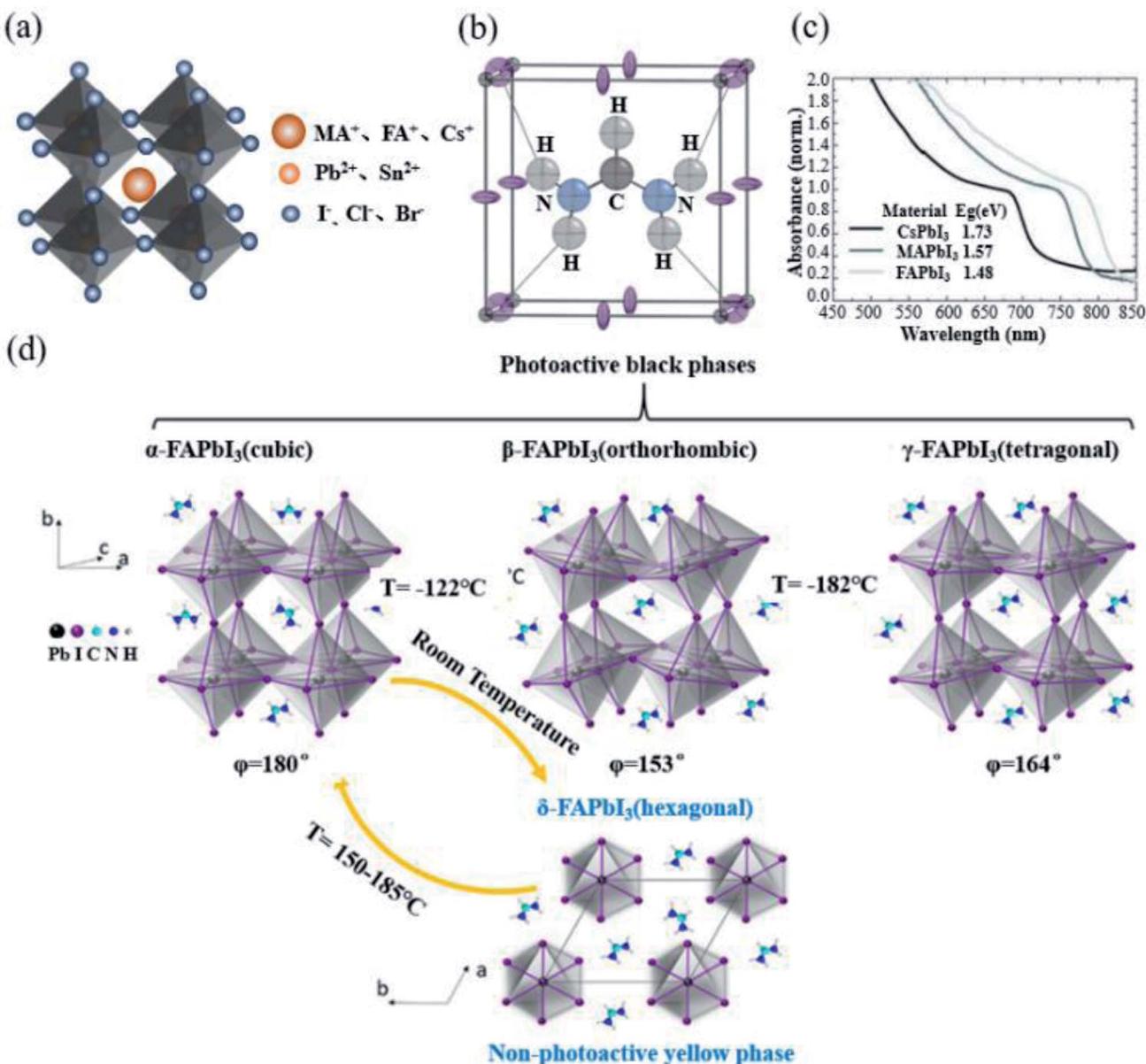
Fig. 2   (a) Schematic diagram of the crystal structure of perovskites. (b) Unit cell structure of α-FAPbI$_3$ at 298 K. The dark gray, purple, black, blue, and pale gray spheres correspond to the Pb, I, C, N, and H atoms. NH−I hydrogen bonds are shown as dotted lines. Reprinted with permission from ref. 53, copyright 2015, American Chemical Society. (c) UV-Vis spectra for the APbI$_3$ perovskites formed, where A is either cesium (Cs), MA or FA. Reprinted with permission from ref. 18, copyright 2014, The Royal Society of Chemistry. (d) Crystal structure of the FAPbI$_3$ perovskite and phase transition between each crystal form. The common crystal structure of FAPbI$_3$ involves mainly α and δ phases, and β and γ phases are formed at extremely low temperatures. Reprinted with permission from ref. 54, copyright 2020, American Chemical Society.

Table 3 Basic material performance comparison of α-FAPbI$_3$ and MAPbI$_3$

Name	Band gap (eV)[7,15]	Cation radius of A (pm)[15,45]	Tolerance factor[45]	Effective mass[47]		Carriers mobility (cm^2 V^{-1} s^{-1})[50]		Diffusion length (μm)[50]		Cation reorientation rate (ps)[48,49]	Hydrogen vacancies total capture coefficient (cm^3 s^{-1})[52]
				e	h	e	h	e	h		
MAPbI$_3$	1.55	217	0.91	0.19m_e	0.25m_h	2–40	10–44	2–8	1.8–12	108 ± 18 (300 K)	3.2×10^{-8}
α-FAPbI$_3$	1.48	253	0.99	0.18m_e	0.23m_h	—	35	6.6	—	8.7 ± 0.5 (294 K)	0.8×10^{-4}

and 0.25m_h, while the effective masses of holes and electrons of FAPbI$_3$ are slightly smaller than 0.18 m_e and 0.23 m_h.[47] Generally, the smaller the effective mass is, the faster the carrier mobility will be. J. Kubicki *et al.* used ^{14}N, ^{2}H, ^{13}C, and ^{1}H solid-state MAS NMR magnetic resonance (NMR) to elucidate the cation reorientation dynamics of (MA)$_x$(FA)$_{1-x}$PbI$_3$ between 100 and 330 K. The reorientation rate of the FA cation in the lattice was found to be much higher (8.7 ± 0.5 ps) than that of the MA cation (108 ± 18 ps). Faster rotation results in a better orbital overlap, and it is easier to form polarons, so electrons overcome recombination more effectively.[48,49] The carrier mobility and diffusion length of FAPbI$_3$ are similar to those of MAPbI$_3$.[50] The hydrogen vacancy total capture coefficient of MAPbI$_3$ and α-FAPbI$_3$ is 3.2×10^{-8} cm^3 s^{-1} and 0.8×10^{-4} cm^3 s^{-1}, and H vacancy in FAPbI$_3$ has a higher formation energy than that of MAPbI$_3$. Compared with MA cations, the use of organic FA cations has greater chemical thermal stability and evaporation resistance.[16] Table 3 presents the summary of the inherent properties of α-FAPbI$_3$ and MAPbI$_3$.[51]

The combination of polar materials, high masses, and therefore, low phonon energies and fairly decent densities of deep defects is a desirable condition for slow non-radiative recombination. For α-FAPbI$_3$ perovskite materials, fairly large defect densities that are not midgap should be tolerable as long as there is no trap-to-trap transition possible. In 2015, Derezis *et al.* found that perovskites would also decompose due to the molecular defects in the absence of water and heating in MAPbI$_3$. They speculated that the hydrogen iodide (HI) vacancies caused by volatile HI on the surface broke the thermodynamic equilibrium of the structure.[55] Later, researchers believed that the I-rich environment is a key factor in achieving high-efficiency solar cells.[37] However, in an iodine-rich environment, it was discovered that iodine interstitial is a non-radiative recombination center.[56] In order to understand how far the defect tolerance range of the lead halide perovskite is, Yavari *et al.* deliberately added BiI$_3$ to the precursor solution. They attributed the significant drop in the device performance to the introduction of effective recombination centers by Bi.[57] In 2020, Zhang *et al.* used rigorous first-principles calculations to demonstrate that Bi acts as a donor, and pushes the Fermi level closer to the conduction band; this shift promotes the formation of iodine interstitials, which are the actual nonradiative recombination centers.[58] In 2021, Zhang *et al.* found that the H vacancy has been ignored. They explicitly reveal that the non-

radiative capture coefficient of hydrogen vacancy is 10^{-4} cm^3 s^{-1} by first-principles calculations, four orders of magnitude higher than that of I. Further research found that the H vacancy in FAPbI$_3$ has a higher formation energy compared with MAPbI$_3$. The dissociation energy of the N–H (C–H) bond in MA is lower than that of the N–H (C–H) bond in FA by 0.9 eV (0.4 eV), which implies that FA is intrinsically more stable than MA.[52]

However, FAPbI$_3$ is inferior for its phase stability.[21,23,27,31,38,59] FAPbI$_3$ mainly has four different crystal structures, of which the common crystal forms are α-FAPbI$_3$ and non-perovskite phase (δ-FAPbI$_3$). Distortions with the [PbI$_6$]$^{4-}$ octahedra promote the formation of lowered-symmetry β-FAPbI$_3$ and γ-FAPbI$_3$ black phases, as the temperature decreases (Fig. 2d).[54] For α-FAPbI$_3$, it corresponds to the $Pm\bar{3}m$ space group.[60] The C–H in the FA cation points directly to the surface of the cube. The position of a planar formamidinium cation within this cubic framework was energy-minimized *via* density functional theory (DFT, PBEsol functional) within the regular 6.36 Å cube and found to adopt an orientation with the N–CH–N molecular ion fragment lying in the unit cell midplane, the (200) plane, with the C–H bond pointing directly toward the cube face (thereby minimizing CH⋯I interactions) and the C–N bonds directed toward adjacent cube faces. This allows the –NH$_2$ groups to be orientated toward the unit cell edges with the potential formation of NH⋯I hydrogen bonds.[53] For δ-FAPbI$_3$, it corresponds to the $P6_3/mmc$ space group at room temperature. Compared with α-FAPbI$_3$, the yellow non-perovskite δ-FAPbI$_3$ has a larger band gap and poor charge transport, which has an adverse effect on PSCs.[61] Unfortunately, α-FAPbI$_3$ can only be obtained at a high temperature (160 °C). The energy barrier for the conversion of α-FAPbI$_3$ to δ-FAPbI$_3$ obtained at high temperatures is 0.6 eV.[62] However, due to the presence of highly polar ionic bonds, water will cause a large number of defects on the surface of the device, thereby greatly reducing the transformation energy barrier and accelerating the transition rate to δ-FAPbI$_3$.[63] The irreversible degradation product from the thermal degradation of FA was sym-triazine, but it was only probed by the mass spectrometry technique above 95 °C.[16] Recently, it has been discovered that light induced FA$^+$ degradation process in the perovskite precursor solution, and the –CH=NH double bonds of FA$^+$ ions are oxidized to –CH=O double bonds as an irreversible degradation process.[64] Deng *et al.* showed that a slight excess of FAI cannot further improve the efficiency, but can greatly alleviate

the expansion process to improve the photostability of FA-based perovskites.[65]

2.2 Strategies to stabilize α-FAPbI3

As we have seen, FAPbI$_3$ perovskite materials have been mainly used in high-efficiency devices in recent years. The essential idea is to generate α-FAPbI$_3$ and avoid the generation of δ-FAPbI$_3$.

2.2.1 A-site doping. FAPbI$_3$ has a wider absorption range and a more suitable band gap than those of MAPbI$_3$, which makes it promising to obtain a higher efficiency than that of MAPbI$_3$, but the conditions for obtaining α-FAPbI$_3$ are more rigorous.[17] The difference in the structure and photoelectronic properties of MAPbI$_3$ and FAPbI$_3$ may be due to the difference in the ionic radius between MA (1.8 Å) and FA (1.9–2.2 Å) ions.[21] As the FA$^+$ ion is too large, which makes the lattice unstable, the researchers consider using some cations such as MA$^+$, Cs$^+$, and Rb$^+$ with a smaller ion radius than that of FA$^+$ to partially replace FA$^+$.[19,21–23,27,38] In this way, the tolerance factor can be effectively adjusted to maintain the stability of the α phase, thereby obtaining a high-efficiency device. At the same time, single perovskites (MAPbI$_3$ and FAPbI$_3$) have more intrinsic defects due to their inherent thermal and phase instability.[24]
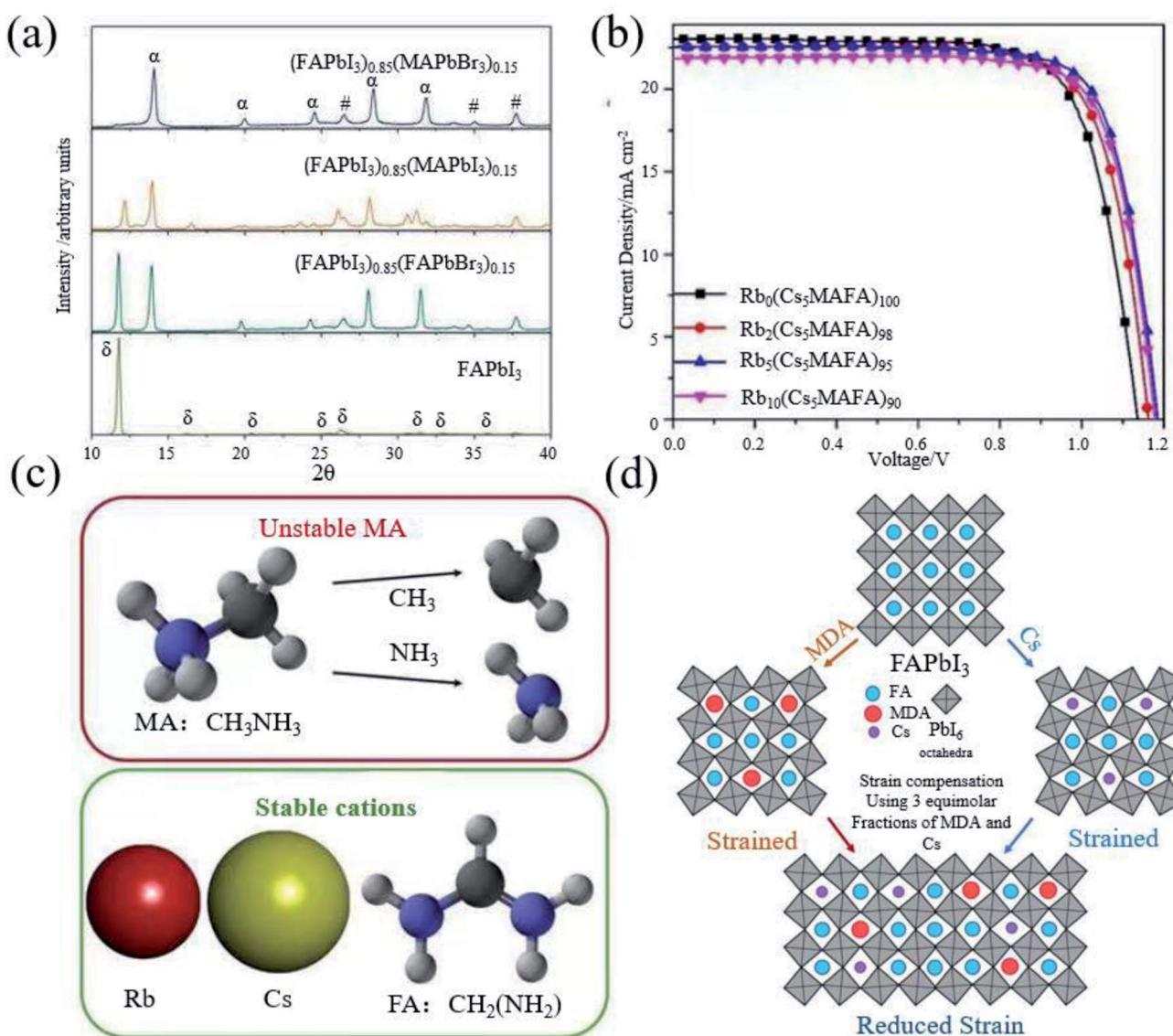

Fig. 3 (a) XRD spectra of solvent-engineering-processed FAPbI$_3$, (FAPbI$_3$)$_{1-x}$(MAPbI$_3$)$_x$, (FAPbI$_3$)$_{1-x}$(FAPbBr$_3$)$_x$, and (FAPbI$_3$)$_{1-x}$(MAPbBr$_3$)$_x$, respectively. Reprinted with permission from ref. 21, copyright 2015, Nature Publishing Group. (b) J–V test of Rb$_0$(Cs$_5$MAFA)$_{100}$PbI$_3$, Rb$_2$(Cs$_5$MAFA)$_{98}$PbI$_3$, Rb$_5$(Cs$_5$MAFA)$_{95}$PbI$_3$, and Rb$_{10}$(Cs$_5$MAFA)$_{90}$PbI$_3$, respectively. Reprinted with permission from ref. 23, copyright 2016, Science Publishing Group. (c) Illustration of the volatile nature of the MA molecule (the I atom is omitted for simplicity), by contrast, Rb, Cs, and FA are thermally more stable cations. Reprinted with permission from ref. 38, copyright 2018, Science Publishing Group. (d) Schematic diagram of the distribution of FA, MDA and Cs in the perovskite crystal lattice, by adding 3 : 3 equimolar fractions of MDA and Cs cations to the perovskite crystal to compensate for the lattice strain. Reprinted with permission from ref. 28, copyright 2020, Science Publishing Group.

Grätzel *et al.* introduced FA^+ in $MAPbI_3$, which makes the absorption edge redshift to increase the absorption range, resulting in a higher short circuit current density.[19] However, the device performance is still inferior due to the component dominated by $MAPbI_3$. Seok *et al.* found that addition of a small amount of $MAPbBr_3$ to $FAPbI_3$ can stabilize the α-$FAPbI_3$ phase (Fig. 3a), contributing to a more uniform morphology and better crystallization.[21] The introduction of Cs also leads to the dominance of $FAPbI_3$, achieving a efficiency of 16.5%.[22] In addition, from the term of the tolerance factor, it has also been found that the mixed cation structure increases the energy and mixed entropy contribution, resulting in a decrease in free energy, thereby improving the stability.[66] Based on this, Grätzel *et al.* began to use ternary mixed perovskite materials ($Cs_{0.5}$($MA_{0.17}FA_{0.83})_{95}Pb(I_{0.83}Br_{0.17})_3$).[24] Soon after, rubidium (Rb) belonging to the same group of Cs was also introduced into the mixed perovskite.

Although $RbPbI_3$ cannot form a black perovskite phase, a small amount of Rb can stabilize α-$FAPbI_3$ and improve the performance to 21.6% (Fig. 3b).[23] It has been found that all the devices containing MA severely degraded after the perovskite devices were annealed for 3 h, although the doping of MA can effectively stabilize α-$FAPbI_3$. It has also been found that the doping of Br will obviously lead to a larger band gap, which reduces the photovoltaic performance of the perovskite.[66] Therefore, it is imperative to make perovskite materials free from MA and Br. Therefore, Saliba *et al.* prepared a $Rb_{0.05}Cs_{0.1}FA_{0.85}PbI_3$ perovskite, without using MA and Br.[38] At the same time, PMMA was used to passivate the surface of the perovskite, so as to obtain an efficiency of 20.35% (Fig. 3c). Methylenediammonium (MDA) has also been introduced to stabilize α-$FAPbI_3$ in recent years due to its ionic radius similar to FA^+. As it has more H atoms and can form more hydrogen bonds with I, only a very small amount of MDA is required. The MDA can achieve the effect of stabilizing the perovskite.[27] Cs was introduced to reduce the local tensile and compressive strains in the perovskite lattice (Fig. 3d), and a certified efficiency of 24.4% was obtained.[28] However, for mixed cationic systems, FA/MA, due to the thermal instability of MA of multi-element cationic mixed perovskites, phase separation will inevitably occur due to the tilt, deformation, expansion and contraction of the octahedral network, local strain may increase consequently, and the short circuit current density will reduce due to the narrowing down of the light-absorption range.[44,66–68] Even though PSCs based on $FA_{0.9}Cs_{0.1}PbI_3$ exhibit reasonable thermal stability, exposure to 1 sun light can cause significant degradation after hundreds of hours of operation.[69]

2.2.2 Additives. Mixed cations will inevitably develop towards a single cation in the future, because the simple components are good for device stability. Therefore, in order to obtain stable single α-$FAPbI_3$, we focus on the additives that are indispensable in the currently used high-efficiency devices. Generally speaking, we hope that the addition of additives can stabilize α-$FAPbI_3$ and improve crystallization, while it will volatilize during the process of annealing to avoid remaining in the perovskite at the same time.

A small amount of HI added to the perovskite precursor solution with a stoichiometric ratio of FAI to PbI_2 of 1 : 1 can assist to form a very uniform and continuous film with high phase purity.[18] Yang *et al.* also introduced thiocyanate (SCN^-) into the $FAPbI_3$ system by adding ammonium thiocyanate (NH_4SCN) into the precursor solution. They found that addition of 30% NH_4SCN can not only improve the water stability, but also promote the generation of α-$FAPbI_3$ and inhibit the generation of δ-$FAPbI_3$ simultaneously. It was found that there was still a small amount of SCN^- in the perovskite, which is attributed to the strong interaction between SCN^- and Pb^{2+} (Fig. 4a). In addition, NH_4SCN mostly evaporates by the end of the annealing process.[70] Xu *et al.* invented a facile bi-additive method (BA method) using HI and $Pb(SCN)_2$ as dual additives to form a new FAI–$Pb(SCN)_2$–HI–*N,N*-dimethylformamide (DMF) intermediate to induce the transition of δ-$FAPbI_3$ to α-$FAPbI_3$.[73] The Lewis acid–base addition method has been widely used to form a uniform perovskite film, which provides a methodological basis for the development of high-performance PSCs. Dimethyl sulfoxide (DMSO) is commonly used as an additive for preparing $FAPbI_3$ and the resulting film is mainly δ-$FAPbI_3$. *N*-Methylpyrrolidone (NMP) avoids the formation of the δ-$FAPbI_3$ phase by forming a more stable mesophase than DMSO, thereby obtaining a pure α-$FAPbI_3$ phase film (Fig. 4b and c).[71,74] The ionic liquid can be used to stabilize α-$FAPbI_3$ by adjusting the crystallization kinetics of the perovskite active layer. 1-Hexyl-3-methylimidazolium iodide ionic liquid (IL) doping is beneficial to $FAPbI_3$ (Fig. 4d). The high polarity and high boiling point of the crystal grains are coarsened, which yields liquid domains between neighbouring grains to reduce the activation energy of the grain-boundary migration.[72]

Cl^- has been demonstrated to improve the crystallization and reduce the non-radiative recombination of perovskites.[59,71,75–77] Methylenediammonium dichloride ($MDACl_2$),[27,28] $MACl$[29] and $FACl$[78] have already been introduced into α-$FAPbI_3$. MACl is considered to be a transitional "stabilizer" that does not affect the crystal structure, and can induce the formation of α-$FAPbI_3$.[79] In addition, it has a good synergistic effect with the commonly used solvent DMSO.[80] In order to reveal the specific mechanism of MACl effected on $FAPbI_3$, Kim *et al.* conducted that the grain size of the perovskite film is directly related to the amount of MACl and the grain size is as high as 1.5 μm with 40% MACl added.

Moreover, compared with the control device without MACl, the roughness of the film reduced from 64.7 nm to 24.7 nm with the addition of 40% MACl. MA has a certain substitution for FA (Fig. 4e), but no Cl is detected, indicating that Cl does not affect the composition of the perovskite, which avoids the discontinuity of perovskite crystallization. The addition of 40% MACl can affect the formation of the α-$FAPbI_3$ structure before the annealing step, and the stable mesophase can be induced to ultra-pure α-phase perovskite after the annealing step. The DFT calculation further proves that Cl can enhance the interaction between FA and I, which helps to improve the stability of the $FAPbI_3$ perovskite. The $FAPbI_3$ device with 40% MACl obtained a certified efficiency of 23.48%.[29] Recently, Jeong *et al.* have
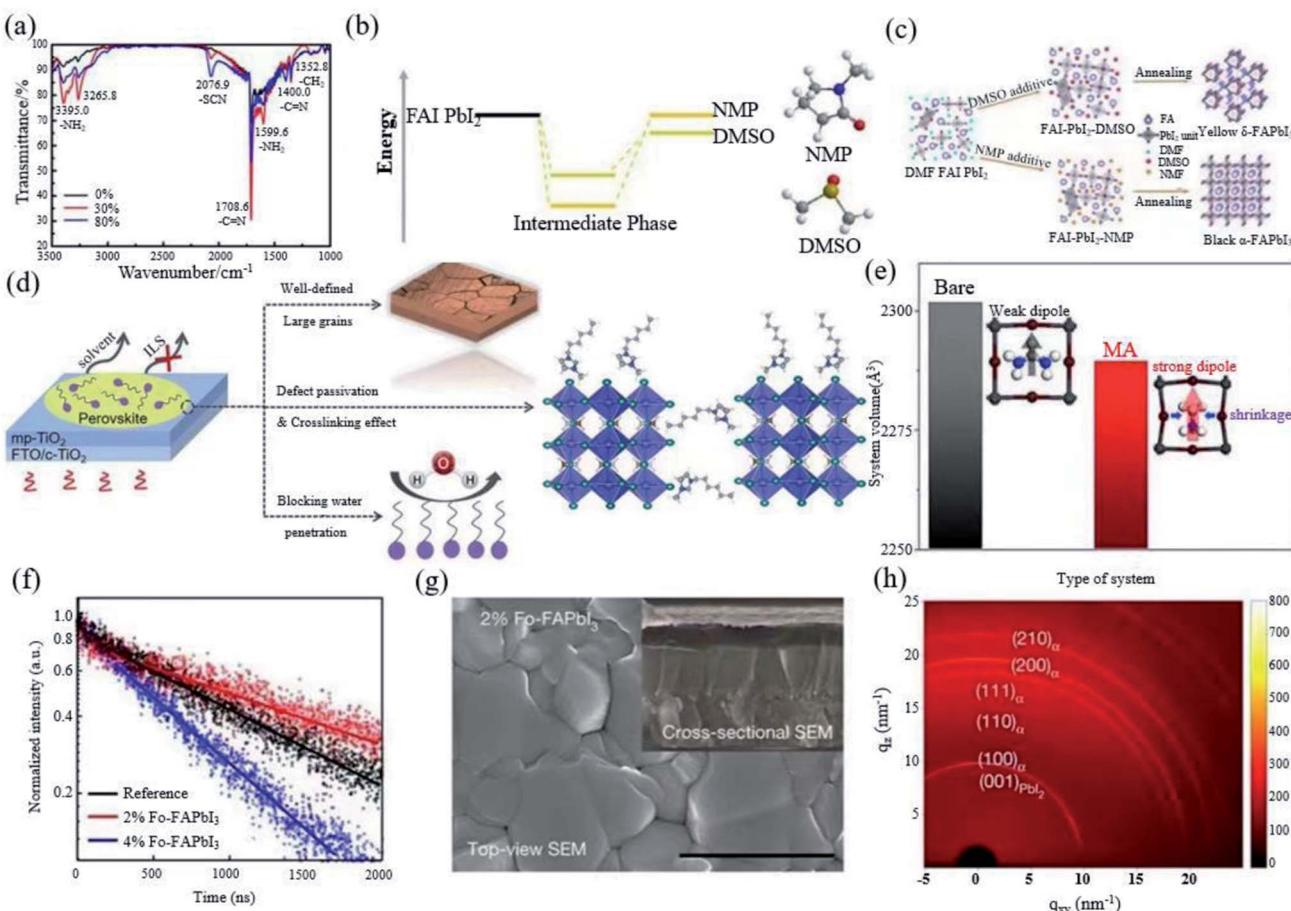
Fig. 4 (a) Fourier transform infrared spectra of FAPbI$_3$ perovskite films with and without SCN$^-$. Reprinted with permission from ref. 70, copyright 2016, The Royal Society of Chemistry. (b) Comparison of the interaction energy of an adduct formed between FAI, PbI$_2$ and DMSO as the Lewis base and that of the related adduct formed with NMP as the Lewis base. (c) Schematic of a blade-coated perovskite film with DMSO or NMP additives. Reprinted with permission from ref. 71, copyright 2020, Advanced Energy Materials. (d) Schematic illustration showing the effects of HMII IL in FAPbI$_3$ active layer. Reprinted with permission from ref. 72, copyright 2020, Advanced Functional Materials. (e) Total volume and cubic-octahedral structure of the bare α-FAPbI$_3$ perovskite structure and that prepared with MA. Reprinted with permission from ref. 29, copyright 2019, Joule. (f) Time-resolved photoluminescence of FAPbI$_3$, 2% Fo-FAPbI$_3$, and 4% Fo-FAPbI$_3$ films, respectively. (g) SEM images of 2% Fo-FAPbI$_3$. (h) Two-dimensional grazing-incidence XRD patterns of 2% Fo-FAPbI$_3$ films. Reprinted with permission from ref. 31, copyright 2021, Nature Publishing Group.

introduced 35% MACl and 2% FAHCOO into the precursor solution. HCOO$^-$ is small enough to fill the I vacancies, thereby reducing the defects. The resulting non-radiative composite (Fig. 4f) increases the voltage and fill factor of the device, and a FAPbI$_3$ perovskite film (Fig. 4g) with improved crystallinity and a larger grain size was obtained. δ-FAPbI$_3$ was not found in synchrotron-based two-dimensional grazing-incidence XRD measurements, which proves that FAHCOO can stabilize the α phase (Fig. 4h), and the device has a certification efficiency of 25.2%.[31]

2.3 From efficiency to stability

The stabilization of α-FAPbI$_3$ *via* cation doping or using additives will more or less cause the perovskite lattice parameters to produce an octahedral tilt, resulting in an increase in the band gap and phase separation, which seriously affects the photovoltaic performance and stability of the PSCs.[69] Therefore, what

we need to consider is to achieve the intrinsic stability of FAPbI$_3$ PSCs, while gaining high efficiency, quantum dot passivation, interface processing and preparation engineering has been tried.

2.3.1 Quantum dots. The introduction of specially designed QDs to passivate the surface of the film can extend the existing composition engineering methods for perovskite films, thereby obtaining high-efficiency PSCs with enhanced stability. In 2019, Que *et al.* used Cs$_{0.57}$FA$_{0.43}$PbI$_3$ QDs to modify the surface of FAPbI$_3$-based perovskite films.[85] The addition of PbS QDs to the perovskite precursor solution has minimal effects on the band gap. It was found that the PbS-FAPI interface reduces the thermodynamic preference for the yellow phase by generating stronger chemical bonds with the black phase and spreading the strain field over a long distance (Fig. 5a), which is conducive to the formation of large-sized grains. These factors indicate that surface chemical engineering is a less invasive but more effective method to stabilize halide perovskite materials.[81]
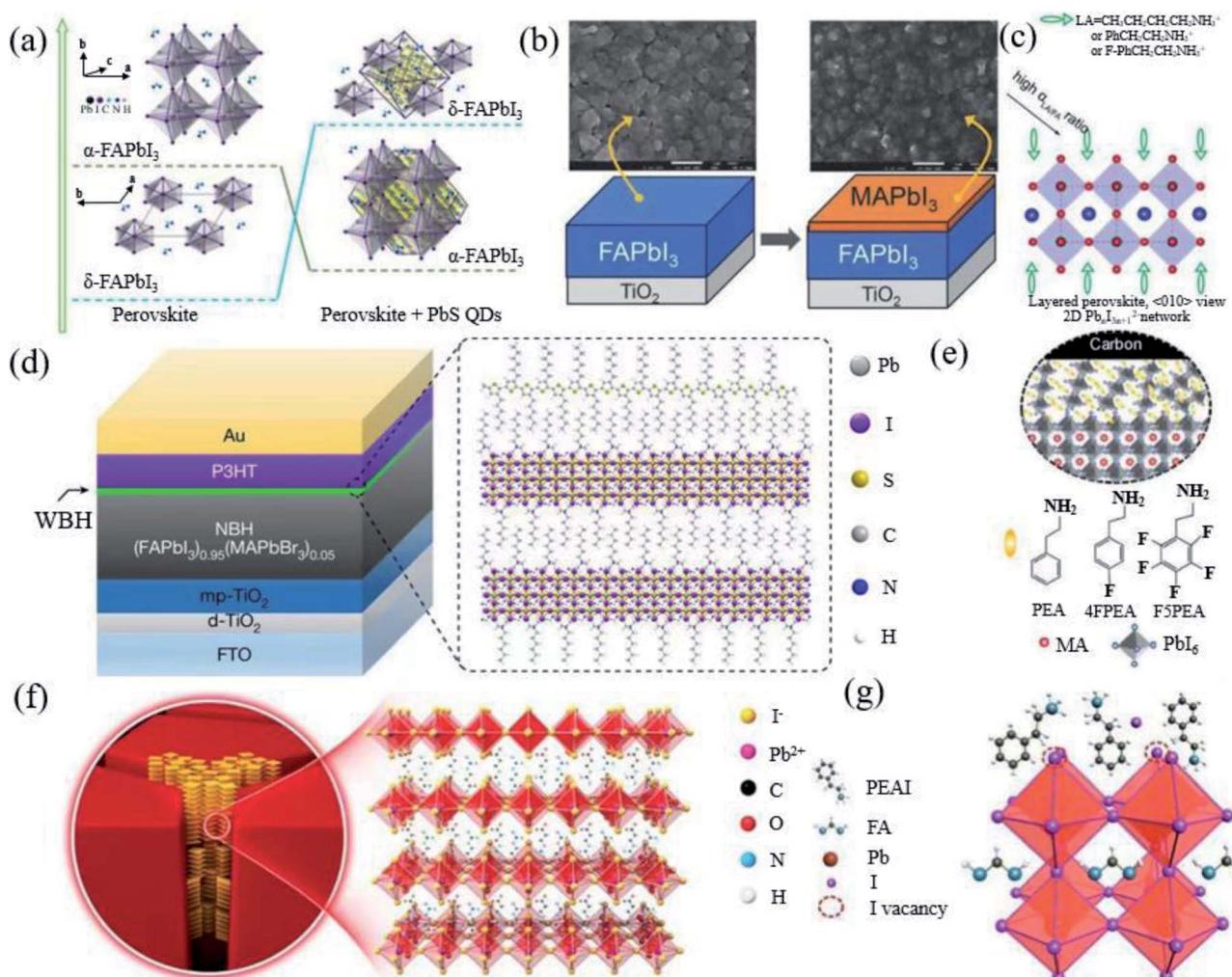
Fig. 5 (a) Interaction process diagram between PbS and FAPbI$_3$. Reprinted with permission from ref. 81, copyright 2020, American Chemical Society. (b) Diagram of MAPbI$_3$ deposited on FAPbI$_3$. Reprinted with permission from ref. 20, copyright 2014, Advanced Materials. (c) Schematic diagram of the long-chain alkyl or aromatic ammonium (LA) cations bound to the surface of the perovskite structure. Reprinted with permission from ref. 82, copyright 2014, Advanced Materials. (d) Diagram of the ultrathin wide-bandgap halide (WBH) stacked onto a narrow-bandgap halide (NBH). Reprinted with permission from ref. 83, copyright 2019, Nature Publishing Group. (e) Interface scheme of F5PEAI at the interface between the 3D perovskite and carbon. Reprinted with permission from ref. 84, copyright 2021, Advanced Energy Materials. (f) Diagram illustrating the crystal structure of the 2D perovskite with $n = 1$. Reprinted with permission from ref. 30, copyright 2020, Advanced Materials. (g) Schematic diagram of the possible passivation mechanism of the PEAI layer of the perovskite film. Reprinted with permission from ref. 26, copyright 2019, Nature Publishing Group.

2.3.2 Interface processing. Defects are most likely to occur at the surface and interface of perovskites, and the passivation of surface defects of PSCs has always been the top priority. Proper interface treatment can effectively reduce non-radiative recombination and increase the open circuit voltage of the device, so as to improve the performance and stability of the device. As early as in 2014, Park *et al.* covered the undoped FAPbI$_3$ with a thin layer of MAPbI$_3$ to improve the performance of the device (Fig. 5b).[20]

Macromolecular polymer polymethyl methacrylate (PMMA) has been reported as a buffer layer to improve the air stability of the device.[38] Long-chain alkyl or aromatic ammonium (LA)-like *n*-butylammonium (*n*-C$_4$H$_9$NH$_3^+$, BA), phenylethylammonium (C$_6$H$_5$CH$_2$CH$_2$NH$_3^+$, PEA), and 4-fluorophenylethylammonium

(4-FC$_6$H$_5$CH$_2$CH$_2$NH$_3^+$, FPEA) iodide have proved that surface functionalization can enable the stabilization of the metastable perovskite phase in pure FAPbI$_3$ without cation or anion alloying (Fig. 5c).[82] The longer alkyl ammonium chain promotes the hydrogen bond with the octahedron and self-assembles to form a new perovskite structure product, thereby stabilizing the FA perovskite. The appropriate amount of LA ions will not enter the perovskite lattice. Surface passivation or the construction of 2D/3D perovskite heterostructures *via* post-processing has also been proven to effectively increase the photovoltage of PSCs. Jung *et al.* used the *in situ* reaction of *n*-hexyl trimethyl ammonium bromide (HTAB) on the surface of the perovskite to form a thin layer of wide-bandgap halide perovskite on top of the narrow-band-gap light absorption layer (Fig. 5d).[83] Jiang *et al.*

formed phenethylammonium iodide (PEAI) on the surface of a 3D perovskite (Fig. 5g).[26] Yao *et al.* used β-guanidinopropionic acid molecules to embed in the grain boundaries of 3D perovskite grains, distributed in half the thickness of the film (Fig. 5f).[30] Chen *et al.* applied pentafluorophenylethylammonium iodide (F5PEAI) to post treat the perovskite/carbon interface (Fig. 5e).[84] These 2D perovskites are all on the surface and grain boundaries of the 3D FAPbI$_3$ crystal lattice. The resulting longer and hydrophobic carbon chain improves the water stability of the perovskite. This may be an effective structural stabilizer (inhibiting lattice deformation) and chemical stabilizer (enhancing the interaction between 3D grains) in FA-based perovskites. Recently, an *in situ* crosslinking-enabled strain-regulating crystallization (CSRC) method with trimethylolpropane triacrylate has been introduced to precisely regulate the top section of the perovskite film, where the largest lattice distortion occurs by Zhang *et al.*[77]

2.3.3 Preparation engineering. As mentioned above, the key to further improve performance lies in how to achieve the stability of pure-phase α-FAPbI$_3$ without doping or using additives. Preparation engineering techniques such as the gas phase method, nano-confined domain, or epitaxial growth method have been employed. Lu *et al.* developed a deposition method using MASCN vapor treatment (Fig. 6a).[86] δ-FAPbI$_3$ was converted into the required pure α-FAPbI$_3$ below the thermodynamic phase transition temperature. This steam treatment only needs 5 s at 100 °C to achieve the preparation of stable α-FAPbI$_3$. Gu *et al.* found that the nano-alumina channel can prevent the transformation of the FAPbI$_3$ perovskite from α to δ phase by restricting the expansion of nanoparticles in the *ab* plane (Fig. 6b).[87] Zhou *et al.* observed the phase transition process of FAPbI$_3$ in mesoporous TiO$_2$ and mesoporous Al$_2$O$_3$ and found that part of the perovskite was encapsulated in the mesopores, which significantly slowed down the phase transition rate. The high contact area increases the barrier for the α–δ transition, thereby stabilizing the α phase (Fig. 6c).[88] The recent work of our group also mentioned this.[89] We found that the printable triple-layer mesoscopic structure localized MAPbI$_3$ on the nanoscale,
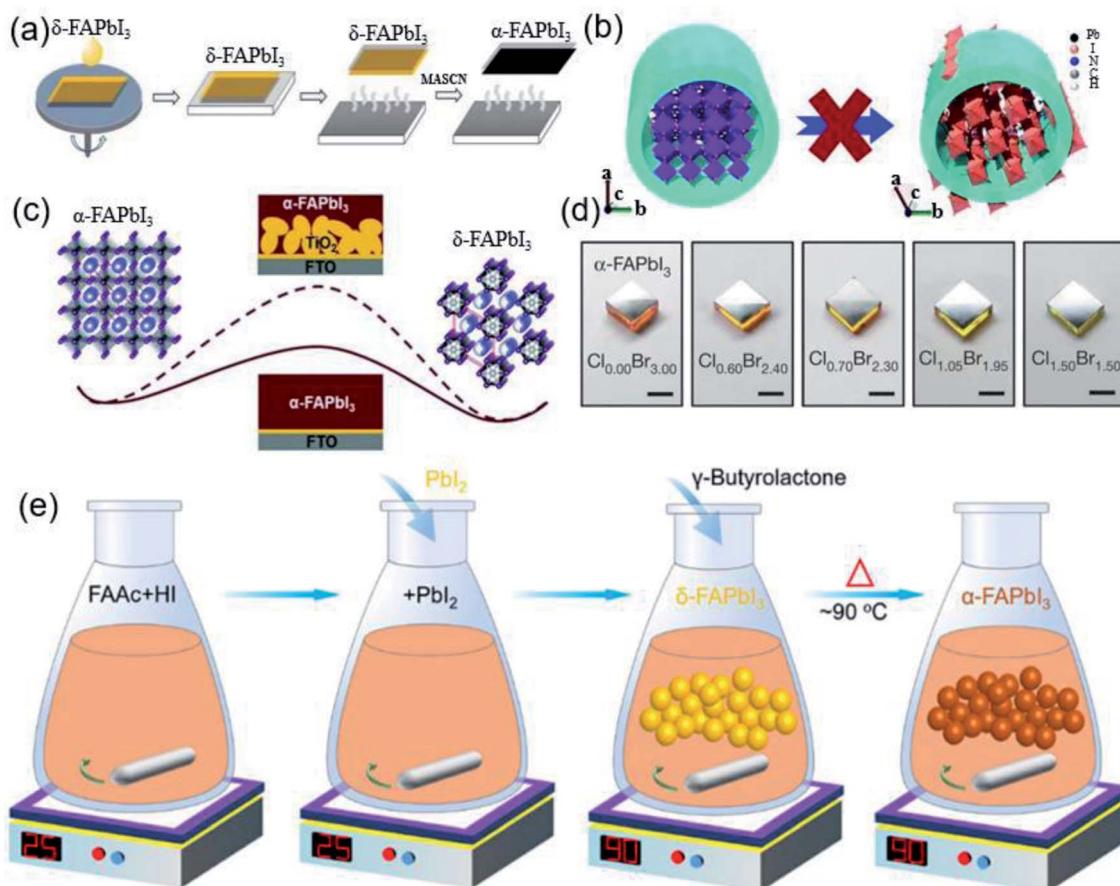

Fig. 6 (a) Simplified scheme of the MASCN vapor treatment process for the pure black-phase FAPbI$_3$ perovskite film. Reprinted with permission from ref. 80, copyright 2020, Science Publishing Group. (b) Schematic of the mechanism of the anodized alumina membrane (AAM) prohibiting the α-to-δ phase transition of FAPbI$_3$ NWs *via* spatial confinement. Reprinted with permission from ref. 81, copyright 2018, The Royal Society of Chemistry. (c) Barrier diagram increment of the α-FAPbI$_3$-to-δ-FAPbI$_3$ transition with the increase in FAPbI$_3$/TiO$_2$ interface area. Reprinted with permission from ref. 82, copyright 2016, The Royal Society of Chemistry. (d) Optical images of α-FAPbI$_3$ epitaxial films grown on different substrates. Reprinted with permission from ref. 84, copyright 2020, Nature Publishing Group. (e) Diagram of a simple method for the synthesis of high-purity FAPbI$_3$ powder to prepare high-efficiency devices. Reprinted with permission from ref. 86, copyright 2019, American Chemical Society.

the decomposition or reconstruction of MAPbI$_3$ was inhibited, and such an effect is hopeful to achieve the stability of pure α-FAPbI$_3$. Chen *et al.* also found a cubic perovskite with a structure similar to α-FAPbI$_3$, and then grew α-FAPbI$_3$ on the surface of this perovskite, so that the atoms in the two perovskite lattices can be aligned, and finally form a false cubic phase (Fig. 6d).[90] Due to the lattice mismatch, the size of the perovskite lattice is smaller than that of α-FAPbI$_3$. Therefore, the α-FAPbI$_3$ lattice is squeezed by compressive stress. The alignment between lattice atoms is called epitaxy, and this epitaxy uses chemical forces to force α-FAPbI$_3$ to maintain a cubic phase, which is consistent with that of the substrate, thereby maintaining stability for at least one year. For α-FAPbI$_3$, the efficiency is constant unless significant phase transition occurs.[91] By using the gas phase method, nano-confined domain, or epitaxial growth, stable α-FAPbI$_3$ can be achieved. Although these methods for FAPbI$_3$-based PSCs are currently rarely studied, we cannot deny that they can provide feasible techniques and inspirations for the realization of pure α-FAPbI$_3$. We found that among the recent articles on high efficiency, some used the method of synthesizing FAPbI$_3$ perovskite powders to replace the original stoichiometric ratio of the precursor solution configuration to prepare perovskite films (Fig. 6e).[92,93] Through this method, unnecessary defects are avoided caused by the uncontrollable stoichiometric ratio. At the same time, a large amount of perovskite powder is synthesized at one time, which greatly improves the repeatability of the device. High-purity PbI$_2$ raw materials are quite expensive, and experiments often fail due to different batches of PbI$_2$. However, the chemically synthesized FAPbI$_3$ powder does not require high purity of raw materials, which further reduces the cost of the device. Compared with the traditional stoichiometric ratio precursor solution, the film made of the FAPbI$_3$ powder has fewer defects, and the FAPbI$_3$ film only needs to be synthesized at room temperature. The "powder method" is considered to be an efficient way to obtain reproducible, high-efficiency, and large-scale production of PSCs. The stability of the perovskite material is a prerequisite. In addition, the further realization of the stability of the perovskite material together with other functional materials in the device structure is the key to realize the stability of the perovskite solar cell.

3. Perspective and outlook

In order to achieve higher efficiency to approach or exceed the S–Q limit, and to look for feasible industry-academia cooperation, we make a perspective and outlook in the future development of FAPbI$_3$ perovskite materials after solving the α-FAPbI$_3$ phase problem.

3.1 Theoretical efficiency

At present, the four parameters of the highest efficiency FAPbI$_3$-based single-junction PSCs (Fo-FAPbI$_3$, E_g = 1.53 eV) are as follows: V_{oc} = 1.174 V, J_{sc} = 26.25 mA cm^{-2}, FF = 0.818, efficiency = 25.21%.[31] The four parameters of solar cells with light absorbers corresponding to a band gap of 1.53 eV calculated by

the S–Q limit are as follows: V_{oc} = 1.243 eV, J_{sc} = 27.99 mA cm^{-2}, FF = 0.901, efficiency = 31.34%.[13] The four parameters of FAPbI$_3$-based PSCs account for 94.4% (V_{oc}), 93.8% (J_{sc}), 90.8% (FF), and 80.4% (efficiency) of the S–Q limit, respectively. We can see that the lowest fill factor (FF) may be responsible for the efficiency loss, and the improvement of FF is usually the most difficult. In PSCs, the resistance element is usually composed of series resistance (R_s) and parallel resistance (R_{sh}). In order to obtain a higher FF, R_s as small as possible and R_{sh} as large as possible are usually required. R_s is related to the resistance of the device materials and resistive contacts, and R_{sh} is caused by the current leakage through the device, such as the body and the interface, the carrier recombination, the contact between the ETL and the HTL, and the leakage around the edge of the device.[94] The improvement of the device efficiency is to further solve the interface contact problem of the device to obtain a higher R_{sh}, thereby obtaining a higher FF. Due to the reduction in the interface recombination, a higher V_{oc} can theoretically be obtained. At present, the band gap of FA-based perovskites is more or less widened due to doping or additive use.

In order to further improve the performance of the device, obtaining pure α-FAPbI$_3$ and obtaining a lower band gap perovskite may be a potential means.

3.2 Band gap adjustment

The band gap of FAPbI$_3$ is 1.48 eV, which has a certain distance with the S–Q limit of 1.34 eV.[95] Therefore, band gap tuning, for example, by mixing halides or making Sn–Pb compounds (Fig. 7a and b) is one of the main ways to improve the efficiency.[40] Both pure Sn and Sn–Pb show better charge transport performance than that of Pb-based perovskites,[96–98] and the highest efficiency reaches 21.74%.[99] Moreover, compared to the voltage loss of Pb-based perovskites, the voltage loss of the Sn–Pb perovskite can now be 0.33 V, which is comparable to that of FAPbI$_3$-based devices.[100] The carrier lifetime has reached more than 1 μs.[101] There are reasons to believe that in the future development, Sn–Pb perovskites can reach a new height.

However, so far, Sn–Pb perovskites have a certain distance from their theoretical efficiency. This is mainly because Sn^{2+} is easily oxidized to Sn^{4+}, which leads to the generation of Sn vacancies. At the same time, the Sn–Pb mixed perovskite also has the problem of phase separation. In the future, there may be better ways to solve this problem and move closer to the S–Q limit.

3.3 Tandem solar cells

In 1961, Shockley and Queisser reported that the theoretical efficiency of a single junction solar cell was 33% *via* calculation.[13] The tandem solar cell is considered to be the most likely means to break the S–Q limit. PSCs exhibit excellent photovoltaic performance, band gap tunability, low temperature and low-cost solution processability, which make them ideal candidates for the preparation of tandem solar cells. The maximum PCE is expected to exceed 40%.[102] There are many types of tandem solar cells, and PSCs have important
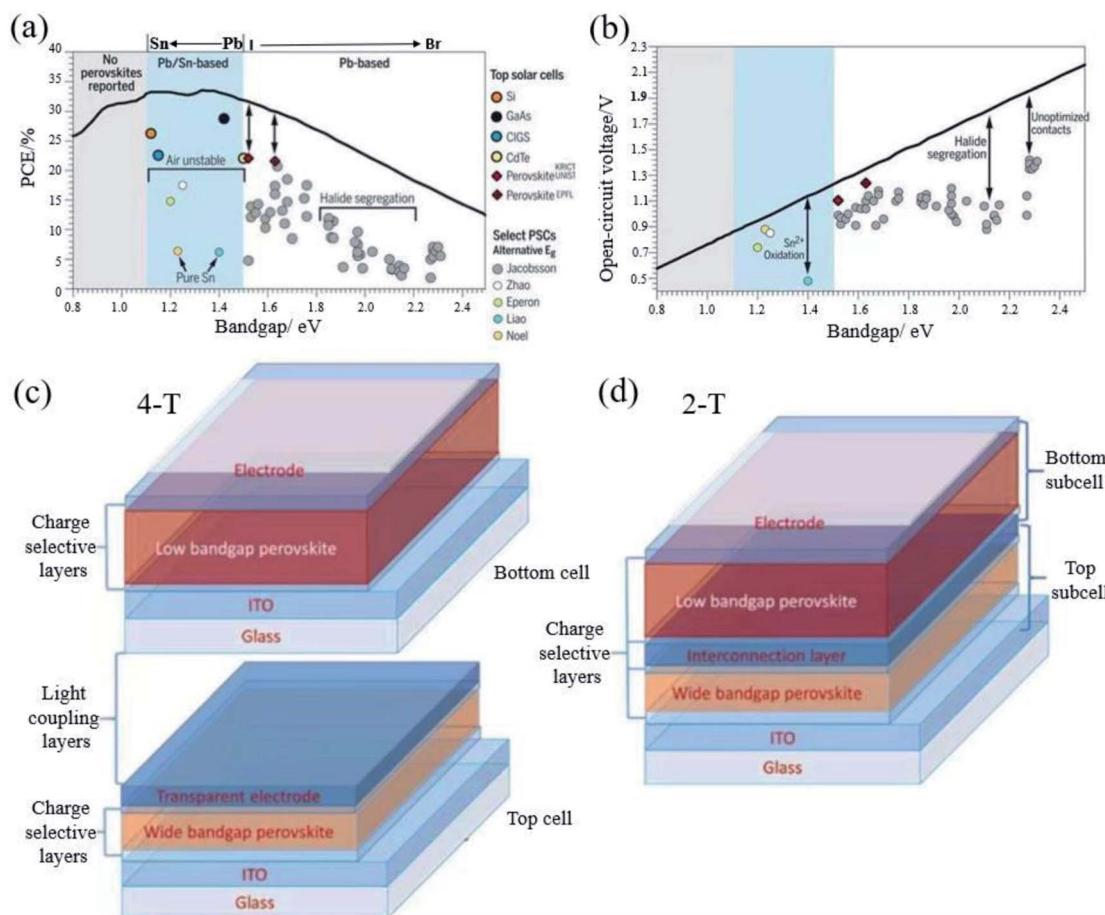
Fig. 7 (a) Shockley–Queisser efficiency and (b) calculated maximum V_{OC} (radiative limit). Reprinted with permission from ref. 32, copyright 2017, Science Publishing Group. Structure diagram of (c) 4-T and (d) 2-T solar cells. Reprinted with permission from ref. 96, copyright 2019, Advanced Functional Materials.

applications in tandem solar cells because of their adjustable band gap and low cost.

Tandem cells mainly have two-terminal (2-T) and four-terminal (4-T) stacking methods (Fig. 7c and d).[102] The 4-T series unit consists of independent wide band gap and narrow band gap devices. 4-T devices are mechanically stacked together, and the two sub-units are manufactured separately and connected by an external circuit. Although the production and operation process of 4-T is relatively simple, the additional two electrodes and corresponding optical loss usually result in high cost.[101] In contrast to 4-T devices, 2-T cells are sequentially fabricated on a single substrate with a transparent front electrode and an opaque back electrode, where the front cell and the back cell are connected by an interconnect layer (ICL). As shown in Fig. 7d, ICL is where the recombination of photo-generated carriers from the front and back sub-cells occurs to maintain charge neutrality in the metal composite layer or the inter-band tunnel junction.[103] 2-T tandem solar cells can avoid additional manufacturing costs and spectrum loss, which make them more promising than 4-T tandem solar cells in practical applications. In 2-T tandem solar cells, because the narrow band gap and wide band gap solar cells are connected in series, the voltage generated by each sub-cell is added. Kirchhoff's law stipulates that the current flowing through each sub-cell must match, which means that the photocurrent is limited by the lower sub-cell current, and the two sets of cells collect different regions of the solar spectrum. In order to obtain a higher efficiency, it is necessary to achieve photocurrent matching under the condition of the maximum power point of each sub-cell, which requires that the band gaps of the bottom cell and the top cell are extremely matched. Due to the limitations of the manufacturing process and electrical coupling operation, manufacturing 2-T cells is practically more challenging than manufacturing 4-T cells and 4-T tandem solar cells. At present, PSCs are mainly composed of perovskite/perovskite tandem solar cells and perovskite/silicon tandem solar cells. Silicon and low band gap perovskites are generally used as bottom cells. For perovskites, Sn is generally doped to narrow the band gap of perovskites. Recently, the highest efficiency of perovskite/perovskite tandem solar cells has reached 25.6%.[104] Perovskite/silicon tandem solar cells even reached 29.15%.[105] A breakthrough of 30% is just around the corner. Long-term stability is an issue that must be paid attention to for tandem PSCs in order to achieve commercialization. Although 4-T is

more expensive than 2-T in terms of production process, the stability of PSCs is still a big problem at present. 4-T tandem solar cells can be replaced with new cells after the perovskite efficiency has decayed. From this perspective, 4-T tandem solar cells are more suitable for commercialization than the 2-T ones.[106] However, for actual operation, the glass, encapsulation materials and junction box in the 4-T can easily account for half or more of the cost of the panel. At the same time, further realizing the large-scale production of PSCs is also the only way to realize the commercialization of tandem cells. Amplifying the laboratory process and realizing the industry-university-research collaboration are vital.

3.4 Lifetime estimation

Limited by the problem of phase stability, there are still big gaps towards the actual work stability referred to International Electrotechnical Commission (IEC)-61265 standards, especially for the pure-phase α-FAPbI$_3$. Consequently, several modification methods were employed to help the device endure the aging tests.

Monica et al. first introduced a FAPbI$_{3(0.85)}$MAPbBr$_{3(0.15)}$-based traditional mesoporous n-i-p device, and the device operated for >1000 h under real outdoor conditions following the ISOS-1 procedures.[107,108] Park et al. further incorporated an ultrathin two-dimensional (2D) perovskite (5-AVA)$_2$PbI$_4$ (5-AVA = 5-ammoniumvaleric acid) layer, acting as a passivation layer between (FAPbI$_3$)$_{0.88}$(CsPbBr$_3$)$_{0.12}$ and the hole transporting

CuSCN layer in the mesoporous n-i-p structure device by forming 2D/3D heterostructures. The encapsulated device maintains 98% of the PCE after 63 days under moisture exposure of about 10% in the darkness.[109] Dai et al. found that unsealed (Cs$_{0.1}$FA$_{0.9}$PbI$_3$)$_{0.9}$(FAPbBr$_3$)$_{0.1}$-based devices retain about 80% and 90% of the initial PCE at 85 °C with 20% relative humidity (RH) after 260 h and at room temperature with 45 ± 5% RH after 1440 h, respectively.[110] Zhao et al. also prepared a 2D/3D-based device using (FAPbI$_3$)$_n$(BA$_2$PbX$_4$) ($n = 60$) as an absorber. They delivered excellent ambient stability with a t_{80} lifetime exceeding 2880 hours without encapsulation and a PCE as high as 20.62%.[111] Sang et al. reported that an edge-encapsulated FAPbI$_{3-X}$Br$_X$-based PSC exhibits only 5.20% degradation during 1000 h maximum power point tracking under simultaneous damp heat (85 °C, 85% RH) and 1 sun light soaking test conditions.[112]

Seok et al. found that PSCs based on FAPbI$_3$ doped with MMDACl$_2$ maintained remarkable stability. As shown in Fig. 8a, the target device retained >90% of the initial PCE after 70 h under high humidity (85% RH, 25 °C), and the device maintained >90% of its initial PCE and exhibited greatly improved thermal stability monitored at 150 °C and ~25% RH (Fig. 8b). The target device also exhibits high photostability, maintaining ~90% of its initial PCE (>23.0%) over 600 h of irradiation (Fig. 8c).[27]

Hao et al. introduced a DMSO molecule process for improving the quality of Cs-(FAPbI$_3$)$_{0.85}$(MAPbBr$_3$)$_{0.15}$, and 1 cm^2 devices retained 90% of the initial PCE after aging for 50
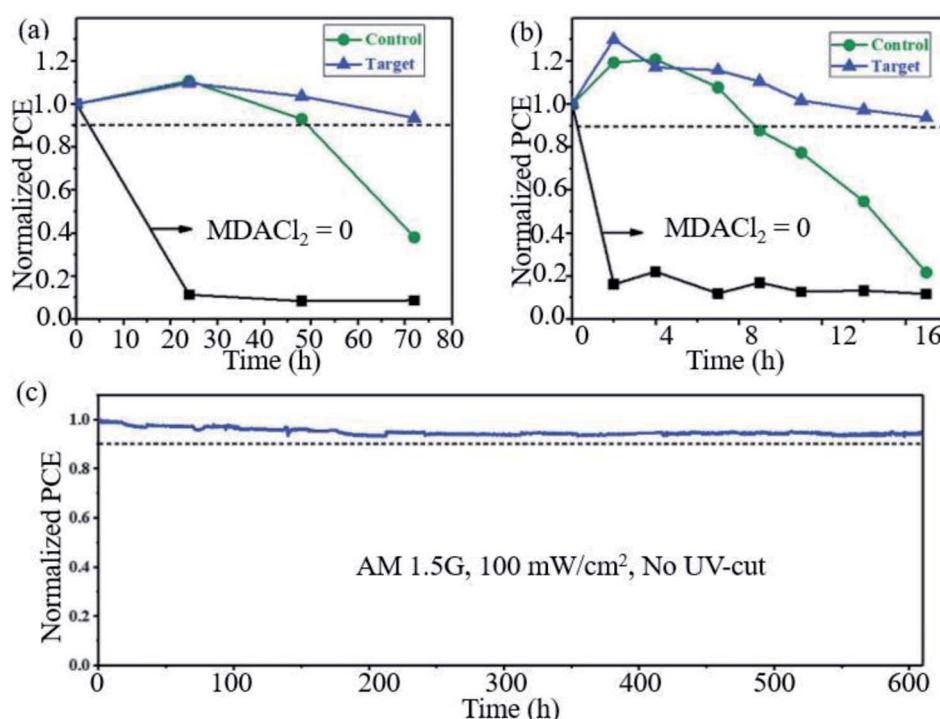

Fig. 8 Long-term stability test. Comparison of (a) humidity (85% RH, 25 °C) and (b) thermal (150 °C, ~25% RH) stability performances of unencapsulated control and target. (c) Maximum power point tracking measured with the encapsulated target device under full solar illumination (AM 1.5G, 100 mW cm^{-2} under ambient conditions) without a UV filter. Reprinted with permission from ref. 27, copyright 2019, Science Publishing Group.
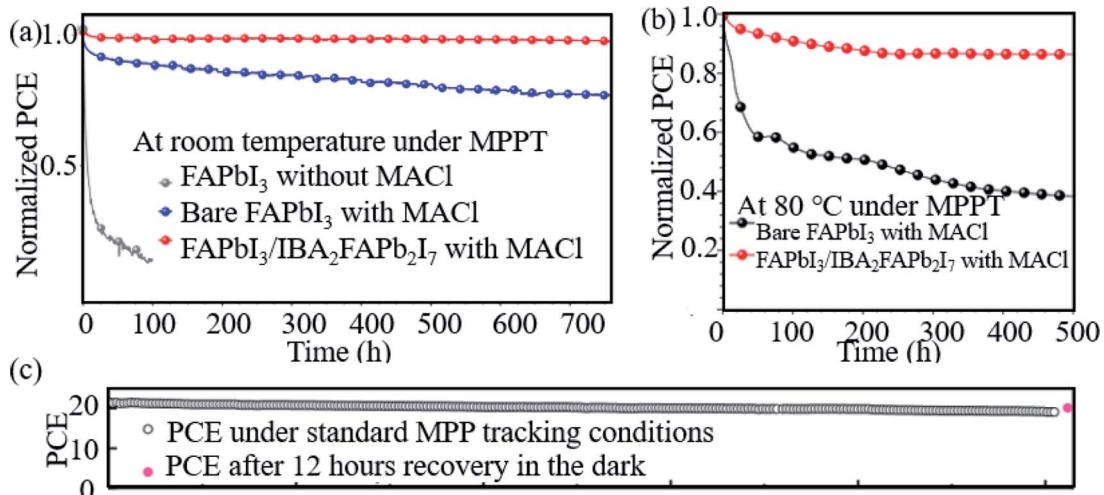
Fig. 9 Aging results (a) and (b) of PSCs based on bare FAPbI$_3$ (black dotted line) and α-FAPbI$_3$/IBA$_2$FAPb$_2$I$_7$ perovskites (red dotted line). Reprinted with permission from ref. 70, copyright 2020, Wiley. (c) Operational stability test of the vapor-treated FAPbI$_3$-based PSCs under 500 hours of MPP-tracking conditions. Reprinted with permission from ref. 80, copyright 2020, Science Publishing Group.

days in ambient air.[113] Zhao *et al.* used a high-energy metastable 2D intermediate of MAFAPbI$_3$Cl to prepare highly crystallized α-FAPbI$_3$ with uniaxial-oriented nature at low temperatures. The unencapsulated device could retain over 95% of its initial PCE after 700 h of illumination, and the champion device could maintain ~19% PCE after storage in a desiccator for 30 days.[114] As shown in Fig. 9a, the 2D/3D IBA$_2$FAPb$_2$I$_7$/α-FAPbI$_3$-based

PSCs reached a PCE close to 23%. The devices retained over 95% and 85% of its initial efficiency under simultaneous exposure with maximum power point tracking (MPPT) to full-simulated sunlight at room temperature and 80 °C over a period of 700 h and 500 h, respectively.[76] Fig. 9c shows that thiocyanate (SCN$^-$)-based vapor-treated α-FAPbI$_3$ PSCs retained 90% of the initial value (21.4%) after 500 hours of MPP measurements, and
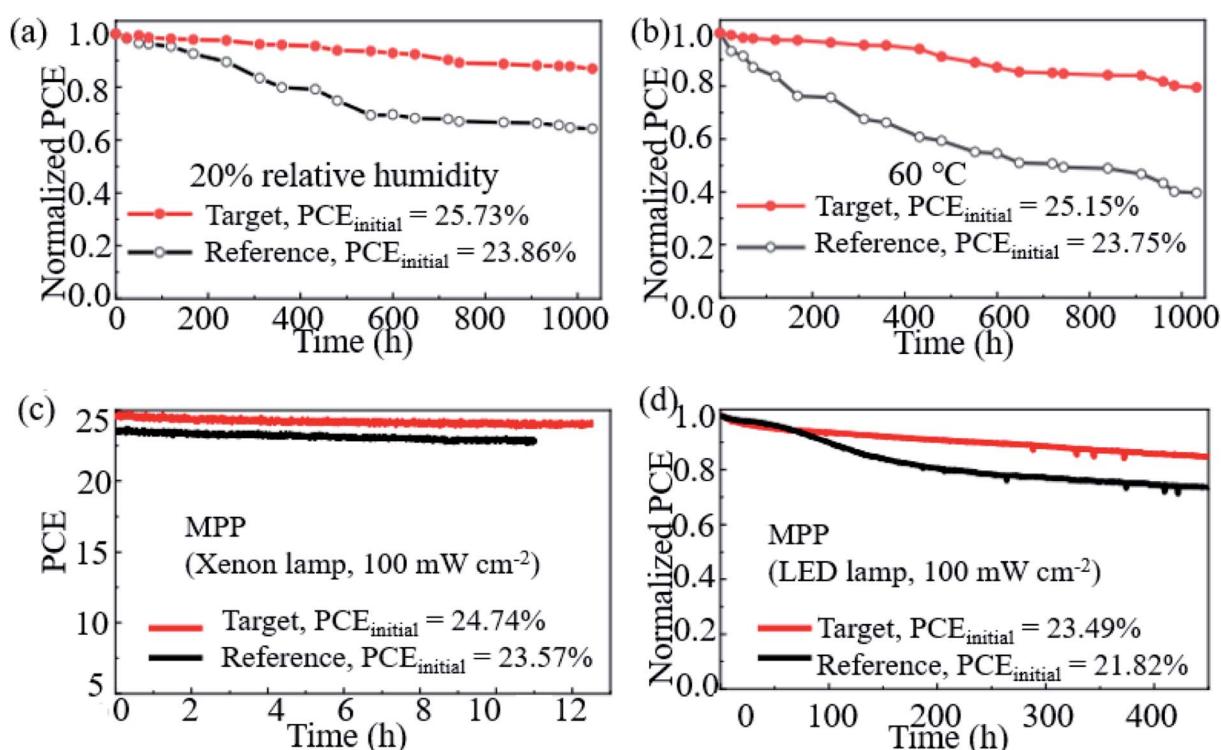

Fig. 10 Stability of the FAPbI$_3$ PSCs. (a) Shelf-life stability of the reference (FAPbI$_3$) and target (FAPbI$_3$ with 2% FAHCOO additive) PSCs. (b) Heat stability of the reference and target PSCs. (c) Operational stability of the reference and target PSCs. (d) Long-term operational stability of the reference and target PSCs. Reprinted with permission from ref. 31, copyright 2021, Nature Publishing Group.

the PCE partially recovered to 20.2%, which is 94.4% of the initial value after 12 h of rest under open-circuit conditions in the darkness.[86] Li *et al.* used a hydrazinium cation (HA$^+$: NH$_2$NH$_3^+$) to obtain novel 1D/3D-based PSCs, and the device retained 90% at room temperature in ambient environment for 2520 h.[115] Kim *et al.* introduced FAPbI$_3$ perovskite films with improved crystallinity and larger grain size by introducing 2% FAHCOO into the precursor solution, and they display that the PCE of the FAPbI$_3$ cells declined by ~35% after 1000 h of aging, whereas FAPbI$_3$ with 2% FAHCOO additive-based cells (target) showed a degradation of only 10% (Fig. 10a). Fig. 10b shows that the target cell retained around 80% of its initial efficiency after 1000 h of aging, whereas the reference cell retained only about 40% at 60 °C under 20% relative humidity. Fig. 10c shows the PCE of the PSCs under continuous light soaking using a xenon lamp. The PCE of the target cell remained above 24% after 10 h MPP tracking, whereas that of the reference cell decreased to 22.8%. Fig. 10d shows that the PCE of the reference cell decreased by about 30%, whereas the target cell lost only around 15% of its initial efficiency.[31] Yan *et al.* further prepared PSCs with remarkable stability. The PSCs triple retained 100% of the initial PCE performance over 104 days under ambient conditions (room temperature, RH = 50 ± 5%) without encapsulation. Han *et al.* innovatively presents that the triple-layer mesoporous structure may provide the nano-confine effect to stabilize pure MA perovskites, Cs/FA perovskites and inorganic pure Cs-based perovskites.[5,116,117] We think that these confined nano structures may also help the stabilization of pure FA-based perovskites.

3.5 Possibility of preparation in ambient air

To further push the advancement to commercialize PSCs, the preparation of PSCs under ambient air conditions even at moderate/high RH will be top priority undoubtedly.

Zhao *et al.* used two-dimensional Ruddlesden–Popper phases to passivate the FAPbI$_3$ perovskite and achieved a PCE as high as 20.62% and remarkable long-term ambient stability with a t_{80} lifetime exceeding 2880 hours without encapsulation (30–40% relative humidity and 25 °C).[111] Jiang *et al.* introduced an *N*-methyl pyrrolidone (NMP) additive-based method to prepare FAPbI$_3$ layers in ambient air under a RH of ~40%, demonstrating the reliability for pure FA-perovskite ambient-air fabrication.[118] Huang *et al.* used methylamine formate to synthesize stable α-FAPbI$_3$ in ambient air regardless of the humidity and temperature, and the unencapsulated cells retain 80 and 90% of their initial efficiencies for 500 hours at 85 °C and continuous light stress.[119] Salim *et al.* also further showed that the long-term stability of NMP additive-pure FAPbI$_3$ PSCs shows a dramatic increase when prepared under ambient air compared to PSCs made under nitrogen.[120] Ma *et al.* incorporated methylamine thiocyanate as a stabilizer, and high-quality and stable α-phase FA-based perovskites in ambient 50 ± 5% RH even at room temperature.[121] Only Huang *et al.*[119] really prepared the FAPbI$_3$ PSCs at high humidity in the atmospheric air and obtained excellent stability. Actually, there are lots of difficulties in the preparation of FAPbI$_3$ perovskites in ambient

air. Maybe the combination of nano-confine effects and ion-liquid additive/solvent methods will do the positive effect for the preparation of FAPbI$_3$ in ambient air, and further to advance the industry.

4. Conclusion

Pure α-FAPbI$_3$ will become the main research focus in the field of perovskite in the future. The key issue is how to eliminate lattice stress and stabilize the pure α-FAPbI$_3$ phase. To further improve the performance and stability of PSCs, we think that a triple-layer mesoporous structure may assist in achieving the stability of perovskites. At the same time, we can continue to explore applications in lower band gaps, such as Sn–Pb PSCs, and also study tandem solar cells to further approach the S–Q limit efficiency. In the future scientific research work, it is necessary to try to use more convenient technical methods, which are easy to scale and make industrialization possible.

Author contributions

Anyi Mei and Hongwei Han designed and directed this paper. Ziwei Zheng and Shiyu Wang wrote this perspective. Yue Hu and Yaoguang Rong revised this manuscript.

Conflicts of interest

There are no conflicts to declare.

Acknowledgements

References

1 H. S. Kim, C. R. Lee, J. H. Im, K. B. Lee, T. Moehl, A. Marchioro, S. J. Moon, R. Humphry-Baker, J. H. Yum, J. E. Moser, M. Gratzel and N. G. Park, *Sci. Rep.*, 2012, **2**, 1–7.

2 J. M. Ball, M. M. Lee, A. Hey and H. J. Snaith, *Energy Environ. Sci.*, 2013, **6**, 1739–1743.

3 J.-Y. Jeng, Y.-F. Chiang, M.-H. Lee, S.-R. Peng, T.-F. Guo, P. Chen and T.-C. Wen, *Adv. Mater.*, 2013, **25**, 3727–3732.

4 K.-C. Wang, J.-Y. Jeng, P.-S. Shen, Y.-C. Chang, E. W.-G. Diau, C.-H. Tsai, T.-Y. Chao, H.-C. Hsu, P.-Y. Lin, P. Chen, T.-F. Guo and T.-C. Wen, *Sci. Rep.*, 2014, **4**, 4756.

5 A. Mei, X. Li, L. Liu, Z. Ku, T. Liu, Y. Rong, M. Xu, M. Hu, J. Chen, Y. Yang, M. Gratzel and H. Han, *Science*, 2014, **345**, 295–298.

6 A. Kojima, K. Teshima, Y. Shirai and T. Miyasaka, *J. Am. Chem. Soc.*, 2009, **131**, 6050–6051.

7 H. Zhou, Q. Chen, G. Li, S. Luo, T.-b. Song, H.-S. Duan, Z. Hong, J. You, Y. Liu and Y. Yang, *Science*, 2014, **345**, 542–546.

8 N. Ahn, D.-Y. Son, I.-H. Jang, S. M. Kang, M. Choi and N.-G. Park, *J. Am. Chem. Soc.*, 2015, **137**, 8696–8699.

9 D.-Y. Son, J.-W. Lee, Y. J. Choi, I.-H. Jang, S. Lee, P. J. Yoo, H. Shin, N. Ahn, M. Choi, D. Kim and N.-G. Park, *Nat. Energy*, 2016, **1**, 16081.

10 S. S. Shin, E. J. Yeom, W. S. Yang, S. Hur, M. G. Kim, J. Im, J. Seo, J. H. Noh and S. I. Seok, *Science*, 2017, **356**, 167–171.

11 W.-Q. Wu, Q. Wang, Y. Fang, Y. Shao, S. Tang, Y. Deng, H. Lu, Y. Liu, T. Li and Z. Yang, *Nat. Commun.*, 2018, **9**, 1–8.

12 K. Wang, C. Wu, Y. Hou, D. Yang, T. Ye, J. Yoon, M. Sanghadasa and S. Priya, *Energy Environ. Sci.*, 2020, **13**, 3412–3422.

13 W. Shockley and H. J. Queisser, *J. Appl. Phys.*, 1961, **32**, 510–519.

14 S. Rühle, *Sol. Energy*, 2016, **130**, 139–147.

15 F. Ma, J. Li, W. Li, N. Lin, L. Wang and J. Qiao, *Chem. Sci.*, 2017, **8**, 800–805.

16 E. J. Juarez-Perez, L. K. Ono and Y. Qi, *J. Mater. Chem. A*, 2019, **7**, 16912–16919.

17 T. M. Koh, K. Fu, Y. Fang, S. Chen, T. C. Sum, N. Mathews, S. G. Mhaisalkar, P. P. Boix and T. Baikie, *J. Phys. Chem. C*, 2013, **118**, 16458–16462.

18 G. E. Eperon, S. D. Stranks, C. Menelaou, M. B. Johnston, L. M. Herz and H. J. Snaith, *Energy Environ. Sci.*, 2014, **7**, 982–988.

19 N. Pellet, P. Gao, G. Gregori, T. Y. Yang, M. K. Nazeeruddin, J. Maier and M. Gratzel, *Angew. Chem., Int. Ed.*, 2014, **53**, 3151–3157.

20 J. W. Lee, D. J. Seol, A. N. Cho and N. G. Park, *Adv. Mater.*, 2014, **26**, 4991–4998.

21 N. J. Jeon, J. H. Noh, W. S. Yang, Y. C. Kim, S. Ryu, J. Seo and S. I. Seok, *Nature*, 2015, **517**, 476–480.

22 J. W. Lee, D. H. Kim, H. S. Kim, S. W. Seo, S. M. Cho and N. G. Park, *Adv. Energy Mater.*, 2015, **5**, 1501310.

23 M. Saliba, T. Matsui, K. Domanski, J. Y. Seo, A. Ummadisingu, S. M. Zakeeruddin, J. P. Correa-Baena, W. R. Tress, A. Abate, A. Hagfeldt and M. Gratzel, *Science*, 2016, **354**, 206–209.

24 M. Saliba, T. Matsui, J.-Y. Seo, K. Domanski, J.-P. Correa-Baena, M. K. Nazeeruddin, S. M. Zakeeruddin, W. Tress, A. Abate and A. Hagfeldt, *Energy Environ. Sci.*, 2016, **9**, 1989–1997.

25 L. Xie, K. Lin, J. Lu, W. Feng, P. Song, C. Yan, K. Liu, L. Shen, C. Tian and Z. Wei, *J. Am. Chem. Soc.*, 2019, **141**, 20537–20546.

26 Q. Jiang, Y. Zhao, X. Zhang, X. Yang, Y. Chen, Z. Chu, Q. Ye, X. Li, Z. Yin and J. You, *Nat. Photonics*, 2019, **13**, 460–466.

27 H. Min, M. Kim, S.-U. Lee, H. Kim, G. Kim, K. Choi, J. H. Lee and S. I. Seok, *Science*, 2019, **366**, 749–753.

28 G. Kim, H. Min, K. S. Lee, D. Y. Lee, S. M. Yoon and S. I. Seok, *Science*, 2020, **370**, 108–112.

29 M. Kim, G.-H. Kim, T. K. Lee, I. W. Choi, H. W. Choi, Y. Jo, Y. J. Yoon, J. W. Kim, J. Lee and D. Huh, *Joule*, 2019, **3**, 2179–2192.

30 Q. Yao, Q. Xue, Z. Li, K. Zhang, T. Zhang, N. Li, S. Yang, C. J. Brabec, H. L. Yip and Y. Cao, *Adv. Mater.*, 2020, **32**, 2000571.

31 J. Jeong, M. Kim, J. Seo, H. Lu, P. Ahlawat, A. Mishra, Y. Yang, M. A. Hope, F. T. Eickemeyer and M. Kim, *Nature*, 2021, **592**, 381–385.

32 J. H. Im, C. R. Lee, J. W. Lee, S. W. Park and N. G. Park, *Nanoscale*, 2011, **3**, 4088–4093.

33 M. M. Lee, J. Teuscher, T. Miyasaka, T. N. Murakami and H. J. Snaith, *Science*, 2012, **338**, 643–647.

34 Y. Wang, W. Chen, L. Wang, B. Tu, T. Chen, B. Liu, K. Yang, C. W. Koh, X. Zhang and H. Sun, *Adv. Mater.*, 2019, **31**, 1902781.

35 W. S. Yang, J. H. Noh, N. J. Jeon, Y. C. Kim, S. Ryu, J. Seo and S. I. Seok, *Science*, 2015, **348**, 1234–1237.

36 D. Bi, C. Yi, J. Luo, J.-D. Décoppet, F. Zhang, S. M. Zakeeruddin, X. Li, A. Hagfeldt and M. Grätzel, *Nat. Energy*, 2016, **1**, 16142.

37 W. S. Yang, B.-W. Park, E. H. Jung, N. J. Jeon, Y. C. Kim, D. U. Lee, S. S. Shin, J. Seo, E. K. Kim and J. H. Noh, *Science*, 2017, **356**, 1376–1379.

38 S.-H. Turren-Cruz, A. Hagfeldt and M. Saliba, *Science*, 2018, **362**, 449–453.

39 M. Jeong, I. W. Choi, E. M. Go, Y. Cho, M. Kim, B. Lee, S. Jeong, Y. Jo, H. W. Choi, J. Lee, J.-H. Bae, S. K. Kwak, D. S. Kim and C. Yang, *Science*, 2020, **369**, 1615–1620.

40 J.-P. Correa-Baena, M. Saliba, T. Buonassisi, M. Grätzel, A. Abate, W. Tress and A. Hagfeldt, *Science*, 2017, **358**, 739–744.

41 A. Miyata, A. Mitioglu, P. Plochocka, O. Portugall, J. T.-W. Wang, S. D. Stranks, H. J. Snaith and R. J. Nicholas, *Nat. Phys.*, 2015, **11**, 582–587.

42 L. M. Herz, *ACS Energy Lett.*, 2017, **2**, 1539–1548.

43 G. Giorgi, J.-I. Fujisawa, H. Segawa and K. Yamashita, *J. Phys. Chem. Lett.*, 2013, **4**, 4213–4216.

44 E. Smecca, Y. Numata, I. Deretzis, G. Pellegrino, S. Boninelli, T. Miyasaka, A. La Magna and A. Alberti, *Phys. Chem. Chem. Phys.*, 2016, **18**, 13413–13422.

45 G. Kieslich, S. Sun and A. K. Cheetham, *Chem. Sci.*, 2014, **5**, 4712–4715.

46 W. Travis, E. Glover, H. Bronstein, D. Scanlon and R. Palgrave, *Chem. Sci.*, 2016, **7**, 4548–4556.

47 A. Amat, E. Mosconi, E. Ronca, C. Quarti, P. Umari, M. K. Nazeeruddin, M. Gratzel and F. De Angelis, *Nano Lett.*, 2014, **14**, 3608–3616.

48 D. J. Kubicki, D. Prochowicz, A. Hofstetter, P. t. Péchy, S. M. Zakeeruddin, M. Grätzel and L. Emsley, *J. Am. Chem. Soc.*, 2017, **139**, 10055–10061.

49 D. J. Kubicki, D. Prochowicz, A. Hofstetter, M. Saski, P. Yadav, D. Bi, N. Pellet, J. Lewiński, S. M. Zakeeruddin and M. Grätzel, *J. Am. Chem. Soc.*, 2018, **140**, 3345–3351.

50 O. Gunawan, S. R. Pae, D. M. Bishop, Y. Virgus, J. H. Noh, N. J. Jeon, Y. S. Lee, X. Shao, T. Todorov and D. B. Mitzi, *Nature*, 2019, **575**, 151–155.

51 J. Y. Kim, J. W. Lee, H. S. Jung, H. Shin and N. G. Park, *Chem. Rev.*, 2020, **120**, 7867–7918.

52 X. Zhang, J.-X. Shen, M. E. Turiansky and C. G. Van de Walle, *Nat. Mater.*, 2021, 1–6.

53 M. T. Weller, O. J. Weber, J. M. Frost and A. Walsh, *J. Phys. Chem. Lett.*, 2015, **6**, 3209–3212.

54 S. Masi, A. F. Gualdrón-Reyes and I. Mora-Sero, *ACS Energy Lett.*, 2020, **5**, 1974–1985.

55 I. Deretzis, A. Alberti, G. Pellegrino, E. Smecca, F. Giannazzo, N. Sakai, T. Miyasaka and A. J. A. P. L. La Magna, *Appl. Phys. Lett.*, 2015, **106**, 131904.

56 X. Zhang, M. E. Turiansky, J.-X. Shen and C. G. Van de Walle, *Phys. Rev. B*, 2020, **101**, 140101.

57 M. Yavari, F. Ebadi, S. Meloni, Z. S. Wang, T. C.-J. Yang, S. Sun, H. Schwartz, Z. Wang, B. Niesen, J. Durantini, P. Rieder, K. Tvingstedt, T. Buonassisi, W. C. H. Choy, A. Filippetti, T. Dittrich, S. Olthof, J.-P. Correa-Baena and W. Tress, *J. Mater. Chem. A*, 2019, **7**, 23838–23853.

58 X. Zhang, J.-X. Shen, M. E. Turiansky and C. G. Van de Walle, *J. Mater. Chem. A*, 2020, **8**, 12964–12967.

59 J. J. Yoo, G. Seo, M. R. Chua, T. G. Park, Y. Lu, F. Rotermund, Y.-K. Kim, C. S. Moon, N. J. Jeon, J.-P. Correa-Baena, V. Bulovic, S. S. Shin, M. G. Bawendi and J. Seo, *Nature*, 2021, **590**.

60 O. J. Weber, D. Ghosh, S. Gaines, P. F. Henry, A. B. Walker, M. S. Islam and M. T. Weller, *Chem. Mater.*, 2018, **30**, 3768–3778.

61 C. C. Stoumpos, C. D. Malliakas and M. G. Kanatzidis, *Inorg. Chem.*, 2013, **52**, 9019–9038.

62 T. Chen, B. J. Foley, C. Park, C. M. Brown, L. W. Harriger, J. Lee, J. Ruff, M. Yoon, J. J. Choi and S.-H. Lee, *Sci. Adv.*, 2016, **2**, e1601650.

63 J. Lin, M. Lai, L. Dou, C. S. Kley, H. Chen, F. Peng, J. Sun, D. Lu, S. A. Hawks and C. Xie, *Nat. Mater.*, 2018, **17**, 261–267.

64 H. Wei, S. Chen, J. Zhao, Z. Yu and J. Huang, *Chem. Mater.*, 2020, **32**, 2501–2507.

65 Y. Deng, S. Xu, S. Chen, X. Xiao, J. Zhao and J. Huang, *Nat. Energy*, 2021, **6**, 633–641.

66 C. Yi, J. Luo, S. Meloni, A. Boziki, N. Ashari-Astani, C. Grätzel, S. M. Zakeeruddin, U. Röthlisberger and M. Grätzel, *Energy Environ. Sci.*, 2016, **9**, 656–662.

67 N. Rolston, K. A. Bush, A. D. Printz, A. Gold-Parker, Y. Ding, M. F. Toney, M. D. McGehee and R. H. Dauskardt, *Adv. Energy Mater.*, 2018, **8**, 1802139.

68 L. Zhang, W. Geng, C.-j. Tong, X. Chen, T. Cao and M. Chen, *Sci. Rep.*, 2018, **8**, 1–9.

69 N. Li, Y. Luo, Z. Chen, X. Niu, X. Zhang, J. Lu, R. Kumar, J. Jiang, H. Liu and X. Guo, *Joule*, 2020, **4**, 1743–1758.

70 S. Yang, W. Liu, L. Zuo, X. Zhang, T. Ye, J. Chen, C.-Z. Li, G. Wu and H. Chen, *J. Mater. Chem. A*, 2016, **4**, 9430–9436.

71 F. Yang, L. Dong, D. Jang, K. C. Tam, K. Zhang, N. Li, F. Guo, C. Li, C. Arrive and M. Bertrand, *Adv. Energy Mater.*, 2020, **10**, 2001869.

72 S. Akin, E. Akman and S. Sonmezoglu, *Adv. Funct. Mater.*, 2020, **30**, 2002964.

73 X. Xu, H. Zheng, G. Liu, L. Zhu, D. He, S. Xu, H. Xu, L. Zhang, X. Zhang and X. Pan, *ChemSusChem*, 2020, **13**, 956–963.

74 J.-W. Lee, Z. Dai, C. Lee, H. M. Lee, T.-H. Han, N. De Marco, O. Lin, C. S. Choi, B. Dunn and J. Koh, *J. Am. Chem. Soc.*, 2018, **140**, 6317–6324.

75 Y. Rong, X. Hou, Y. Hu, A. Mei, L. Liu, P. Wang and H. J. N. c. Han, *Nat. Commun.*, 2017, **8**, 1–8.

76 Y. Liu, S. Akin, A. Hinderhofer, F. T. Eickemeyer, H. Zhu, J. Y. Seo, J. Zhang, F. Schreiber, H. Zhang and S. M. Zakeeruddin, *Angew. Chem., Int. Ed.*, 2020, **59**, 15688–15694.

77 H. Zhang, Z. Chen, M. Qin, Z. Ren, K. Liu, J. Huang, D. Shen, Z. Wu, Y. Zhang, J. Hao, C.-s. Lee, X. Lu, Z. Zheng, W. Yu and G. Li, *Adv. Mater.*, 2021, 2008487.

78 M. Lyu and N.-G. Park, *Sol. RRL*, 2020, **4**, 2000331.

79 C. Mu, J. Pan, S. Feng, Q. Li and D. Xu, *Adv. Energy Mater.*, 2017, **7**, 1601297.

80 J. Qing, X.-K. Liu, M. Li, F. Liu, Z. Yuan, E. Tiukalova, Z. Yan, M. Duchamp, S. Chen, Y. Wang, S. Bai, J.-M. Liu, H. J. Snaith, C.-S. Lee, T. C. Sum and F. Gao, *Adv. Energy Mater.*, 2018, **8**, 1800185.

81 S. Masi, C. Echeverría-Arrondo, K. M. Salim, T. T. Ngo, P. F. Mendez, E. López-Fraguas, D. F. Macias-Pinilla, J. Planelles, J. I. Climente and I. Mora-Sero, *ACS Energy Lett.*, 2020, **5**, 418–427.

82 Y. Fu, T. Wu, J. Wang, J. Zhai, M. J. Shearer, Y. Zhao, R. J. Hamers, E. Kan, K. Deng and X.-Y. Zhu, *Nano Lett.*, 2017, **17**, 4405–4414.

83 E. H. Jung, N. J. Jeon, E. Y. Park, C. S. Moon, T. J. Shin, T. Y. Yang, J. H. Noh and J. Seo, *Nature*, 2019, **567**, 511–515.

84 X. Chen, Y. Xia, Q. Huang, Z. Li, A. Mei, Y. Hu, T. Wang, R. Cheacharoen, Y. Rong and H. J. A. E. M. Han, *Adv. Energy Mater.*, 2021, 2100292.

85 M. Que, Z. Dai, H. Yang, H. Zhu, Y. Zong, W. Que, N. P. Padture, Y. Zhou and O. Chen, *ACS Energy Lett.*, 2019, **4**, 1970–1975.

86 H. Lu, Y. Liu, P. Ahlawat, A. Mishra, W. R. Tress, F. T. Eickemeyer, Y. Yang, F. Fu, Z. Wang and C. E. Avalos, *Science*, 2020, **370**.

87 L. Gu, D. Zhang, M. Kam, Q. Zhang, S. Poddar, Y. Fu, X. Mo and Z. Fan, *Nanoscale*, 2018, **10**, 15164–15172.

88 Y. Y. Zhou, J. Kwun, H. F. Garces, S. P. Pang and N. P. Padture, *Chem. Commun.*, 2016, **52**, 7273–7275.

89 A. Mei, Y. Sheng, Y. Ming, Y. Hu, Y. Rong, W. Zhang, S. Luo, G. Na, C. Tian, X. Hou, Y. Xiong, Z. Zhang, S. Liu, S. Uchida, T.-W. Kim, Y. Yuan, L. Zhang, Y. Zhou and H. Han, *Joule*, 2020, **4**, 2646–2660.

90 Y. Chen, Y. Lei, Y. Li, Y. Yu, J. Cai, M.-H. Chiu, R. Rao, Y. Gu, C. Wang and W. Choi, *Nature*, 2020, **577**, 209–215.

91 V. L. Pool, B. Dou, D. G. Van Campen, T. R. Klein-Stockert, F. S. Barnes, S. E. Shaheen, M. I. Ahmad, M. F. Van Hest and M. F. Toney, *Nat. Commun.*, 2017, **8**, 1–8.

92 G. Tong, D.-Y. Son, L. K. Ono, H.-B. Kang, S. He, L. Qiu, H. Zhang, Y. Liu, J. Hieulle and Y. Qi, *Nano Energy*, 2021, **87**, 106152.

93 Y. Zhang, S. Seo, S. Y. Lim, Y. Kim, S.-G. Kim, D.-K. Lee, S.-H. Lee, H. Shin, H. Cheong and N.-G. Park, *ACS Energy Lett.*, 2019, **5**, 360–366.

94 C. Ma and N.-G. Park, *Chem*, 2020, **6**, 1254–1264.

95 W. Tress, N. Marinova, O. Inganäs, M. K. Nazeeruddin, S. M. Zakeeruddin and M. Graetzel, *Adv. Energy Mater.*, 2015, **5**, 1400812.

96 D. Zhao, C. Chen, C. Wang, M. M. Junda, Z. Song, C. R. Grice, Y. Yu, C. Li, B. Subedi, N. J. Podraza, X. Zhao, G. Fang, R.-G. Xiong, K. Zhu and Y. Yan, *Nat. Energy*, 2018, **3**, 1093–1100.

97 M. Y. Wei, K. Xiao, G. Walters, R. X. Lin, Y. B. Zhao, M. I. Saidaminov, P. Todorovic, A. Johnston, Z. R. Huang, H. J. Chen, A. D. Li, J. Zhu, Z. Y. Yang, Y. K. Wang, A. H. Proppe, S. O. Kelley, Y. Hou, O. Voznyy, H. R. Tan and E. H. Sargent, *Adv. Mater.*, 2020, **32**, 8.

98 X. Jiang, H. Li, Q. Zhou, Q. Wei, M. Wei, L. Jiang, Z. Wang, Z. Peng, F. Wang, Z. Zang, K. Xu, Y. Hou, S. Teale, W. Zhou, R. Si, X. Gao, E. H. Sargent and Z. Ning, *J. Am. Chem. Soc.*, 2021, **143**, 10970–10976.

99 G. Kapil, T. Bessho, T. Maekawa, A. K. Baranwal, Y. Zhang, M. A. Kamarudin, D. Hirotani, Q. Shen, H. Segawa and S. Hayase, *Adv. Energy Mater.*, 2021, 2101069.

100 X. Y. Zhou, L. Z. Zhang, X. Z. Wang, C. Liu, S. Chen, M. Q. Zhang, X. N. Li, W. D. Yi and B. M. Xu, *Adv. Mater.*, 2020, **32**, 8.

101 J. Tong, Z. Song, D. H. Kim, X. Chen, C. Chen, A. F. Palmstrom, P. F. Ndione, M. O. Reese, S. P. Dunfield and O. G. Reid, *Science*, 2019, **364**, 475–479.

102 C. L. Wang, Z. N. Song, C. W. Li, D. W. Zhao and Y. F. Yan, *Adv. Funct. Mater.*, 2019, **29**, 30.

103 R. Lin, K. Xiao, Z. Qin, Q. Han, C. Zhang, M. Wei, M. I. Saidaminov, Y. Gao, J. Xu and M. Xiao, *Nat. Energy*, 2019, **4**, 864–873.

104 K. Xiao, R. Lin, Q. Han, Y. Hou, Z. Qin, H. T. Nguyen, J. Wen, M. Wei, V. Yeddu and M. I. Saidaminov, *Nat. Energy*, 2020, **5**, 870–880.

105 A. Al-Ashouri, E. Köhnen, B. Li, A. Magomedov, H. Hempel, P. Caprioglio, J. A. Márquez, A. B. M. Vilches, E. Kasparavicius and J. A. Smith, *Science*, 2020, **370**, 1300–1309.

106 R. Wang, T. Huang, J. Xue, J. Tong, K. Zhu and Y. Yang, *Nat. Photonics*, 2021, **15**, 411–425.

107 Y. Reyna, M. Salado, S. Kazim, A. Pérez-Tomas, S. Ahmad and M. Lira-Cantu, *Nano Energy*, 2016, **30**, 570–579.

108 M. O. Reese, S. A. Gevorgyan, M. Jørgensen, E. Bundgaard, S. R. Kurtz, D. S. Ginley, D. C. Olson, G. Yaman-Uzunoglu, J.-B. Bonekamp, A. J. J. M. van Breemen, C. Girotto, E. Voroshazi and F. C. Krebs, *Sol. Energy Mater. Sol. Cells*, 2011, **95**, 1253–1267.

109 J. Chen, J.-Y. Seo and N.-G. Park, *Adv. Energy Mater.*, 2018, **8**, 1702714.

110 G. Liu, H. Zheng, L. Zhu, A. Alsaedi, T. Hayat, X. Pan, L. e. Mo and S. Dai, *ChemSusChem*, 2018, **11**, 2436–2443.

111 T. Niu, J. Lu, M.-C. Tang, D. Barrit, D.-M. Smilgies, Z. Yang, J. Li, Y. Fan, T. Luo, I. McCulloch, A. Amassian, S. Liu and K. Zhao, *Energy Environ. Sci.*, 2018, **11**, 3358–3366.

112 J. H. Heo, Y. K. Choi, C. W. Koh, H. Y. Woo and S. H. Im, *Adv. Mater. Technol.*, 2019, **4**, 1800390.

113 X. Liu, L. Shi, J. Huang, Z. Liu, P. Zhang, J. S. Yun, A. M. Soufiani, J. Seidel, K. Sun, Z. Hameiri, J. A. Stride, Y. Zhang, M. A. Green, H. Lin and X. Hao, *Sol. RRL*, 2019, **3**, 1800338.

114 T. Zhang, Q. Xu, F. Xu, Y. Fu, Y. Wang, Y. Yan, L. Zhang and Y. Zhao, *Sci. Bull.*, 2019, **64**, 1608–1616.

115 S. Yu, H. Liu, S. Wang, H. Zhu, X. Dong and X. Li, *Chem. Eng. J.*, 2021, **403**, 125724.

116 X. Hou, M. Xu, C. Tong, W. Ji, Z. Fu, Z. Wan, F. Hao, Y. Ming, S. Liu, Y. Hu, H. Han, Y. Rong and Y. Yao, *J. Power Sources*, 2019, **415**, 105–111.

117 S. Wang, W. Shen, Y. Chu, W. Zhang, L. Hong, A. Mei, Y. Rong, Y. Tang, Y. Hu and H. Han, *J. Phys. Chem. Lett.*, 2020, **11**, 9689–9695.

118 G. Wang, L. Wang, J. Qiu, Z. Yan, K. Tai, W. Yu and X. Jiang, *Sol. Energy*, 2019, **187**, 147–155.

119 W. Hui, L. Chao, H. Lu, F. Xia, Q. Wei, Z. Su, T. Niu, L. Tao, B. Du, D. Li, Y. Wang, H. Dong, S. Zuo, B. Li, W. Shi, X. Ran, P. Li, H. Zhang, Z. Wu, C. Ran, L. Song, G. Xing, X. Gao, J. Zhang, Y. Xia, Y. Chen and W. Huang, *Science*, 2021, **371**, 1359–1364.

120 K. M. Salim, S. Masi, A. F. Gualdrón-Reyes, R. S. Sánchez, E. M. Barea, M. Krečmarová, J. F. Sánchez-Royo and I. Mora-Seró, *ACS Energy Lett.*, 2021, **6**, 3511–3521.

121 J. Zhao, G. He, D. Yang, D. Guo, L. Yang, J. Chen and D. Ma, *Sustainable Energy Fuels*, 2021, **5**, 4268–4276.